Master's thesis

NTNU
Norwegian University of Science and Technology
Faculty of Natural Sciences
Department of Chemical Engineering

Silje Maria Martinsen Tugwell

Evaluation of solvents for upgrading and conditioning of high hydrogen sulphide content biogas to biomethane standards

Master's thesis in Chemical engineering and biotechnology
Supervisor: Hanna Knuutila
Co-supervisor: Diego Di Domenico Pinto
June 2023

NTNU
Norwegian University of
Science and Technology

Silje Maria Martinsen Tugwell

Evaluation of solvents for upgrading and conditioning of high hydrogen sulphide content biogas to biomethane standards

Master's thesis in Chemical engineering and biotechnology
Supervisor: Hanna Knuutila
Co-supervisor: Diego Di Domenico Pinto
June 2023

Norwegian University of Science and Technology
Faculty of Natural Sciences
Department of Chemical Engineering

NTNU
Norwegian University of
Science and Technology

Preface

This thesis was written during the spring semester of 2023 as the final part of my master's degree at the Department of Chemical Engineering in Environmental Engineering and Reactor Technology at the Norwegian University of Science and Technology.

I want to express my appreciation to my external supervisor Diego Di Domenico Pinto, Hovyu for his valuable support and guidance throughout the master's thesis. Also a big thank you to my internal supervisor Hanna Knuutila for guiding me through the thesis and first sparking my interest for chemical engineering 3 years ago in the TKP4100 - Fluid Flow and Heat Transfer course.

I would also like to thank all my friends and loved ones in Trondheim and Milan for making the last five years a most extraordinary experience filled with laughter, tears, and a lot of hours in the study hall. *Grazie di tutto!*

Trondheim, 6th June 2023

Silje Maria Martinsen Tugwell

Table of Contents

List of Figures

List of Tables

List of Acronyms

AAS amino acid salt

AD anaaerobiv digestion

AMP 2- amino-2-methyl-1-propanol

CAPEX Capital Expenditure

CC cyclic capacity

CS carbon steel

CH_4 methane

CHP combined heat and power

CO_2 carbon dioxide

D&E Design and Engineering

DNPV discounted net present value

FC fixed cost

FCC fixed capital cost

GHG greenhouse gas

H_2O water

H_2S hydrogen sulphide

IC inter cooler

ICE internal combustion engine

IEA International Energy Agency

IRR internal rate of return

ISBL inside battery limits

L/G liquid/gas

MEA monoethanolamine

NG natural gas

NPV net present value

OS Offsite

PBT payback time

PFD process flow diagram

PSA pressure swing adsorption

PZ piperazine

SG sodiumglycinate

SRD specific reboiler duty

SS stainless steel

SSC sulphur stress cracking

VC variable cost

VLE vapour-liquid equilibrium

WI Wobbe index

X Contingency

Abstract

There is an increasing interest in production of biogas from biomass with high sulphur content. Removal of CO_2 and H_2S is critical for utilisation of biogas. In this thesis upgrading and conditioning of biogas with high H_2S content (3 mol%) to meet the natural gas grid requirement of 1 mol% CO_2 and 5 mg/mL H_2S was studied.

Simulations with 45 wt% sodium glycinate and 40 wt% CESAR-1 (AMP/PZ: 27/13 wt%) solvents were performed in Protreat. It was found that 45 wt% SG was not able to remove H_2S to meet the natural gas grid standards, furthermore, results from the laboratory showed problems with precipitation. The CESAR-1 solvent was found able to meet the NG grid standards with 15 metre absorption column with a specific reboiler duty of 4.3 MJ/kg acid gas.

The profitability analysis indicated that the cost of acid gas capture with a H_2S inlet concentration of 3 mol% was not economical feasible, but lower inlet concentrations of H_2S were economical where the best case scenario had a payback time of 3 years with a discounted net present value of USD 2.7 million.

Sammendrag

Det er en økende interesse for produksjon av biogass fra biomasse med høyt svovelinnhold. Det er avgjørende å separere ut CO_2 og H_2S før biogassen kan brukes. I denne masteroppgaven ble oppgradering og kondisjonering av biogass med høyt H_2S-innhold (3 mol%) studert for å oppfylle natur gass nettverkskravet på 1 mol% CO_2 og 5 mg/mL H_2S.

Simuleringer med 45 wt% natriumglycinat og 40 wt% CESAR-1 (AMP/PZ: 27/13 wt%) ble gjennomført i simuleringsprogrammet Protreat. Det ble funnet at 45 wt% natriumglycinat ikke var i stand til å fjerne nok H_2S for å oppfylle natur gass nettverksstandarden, i tillegg viste laboratorieeksperimentene problemer med utfelling ved absorpsjon av CO_2. CESAR-1 var i stand til å oppfylle natur gass nettverksstandarden med en 15 meter absorpsjonskolonne og hadde et energiforbruk på 4,3 MJ/kg sur gass i reboileren.

Den økonomiske analysen indikerte at kostnaden for oppgradering og kondisjonering av biogassen med en H_2S konsentrasjon på 3 mol% H_2S ikke er økonomisk gjennomførbart, men caser med lavere konsentrasjoner av H_2S var lønnsomme og det beste tilfelle hadde en tilbakebetalingstid på 3 år med en diskontert netto kontantstrøm på USD 2,7 millioner.

1 Introduction and background

The world's energy demand is in constant increase. The International Energy Agency (IEA) is predicting a 12% growth in energy demand from 2019 to 2030, in a pre-Covid-19 scenario [1], as shown in Figure 1.1 as Pre-crisis trajectory. The figure shows the predicted energy demand from 2018 up until 2030 based on the energy demand in 2019 with an index of 100. This demand for energy needs to be met with an increase in production and development of new and existing energy sources.

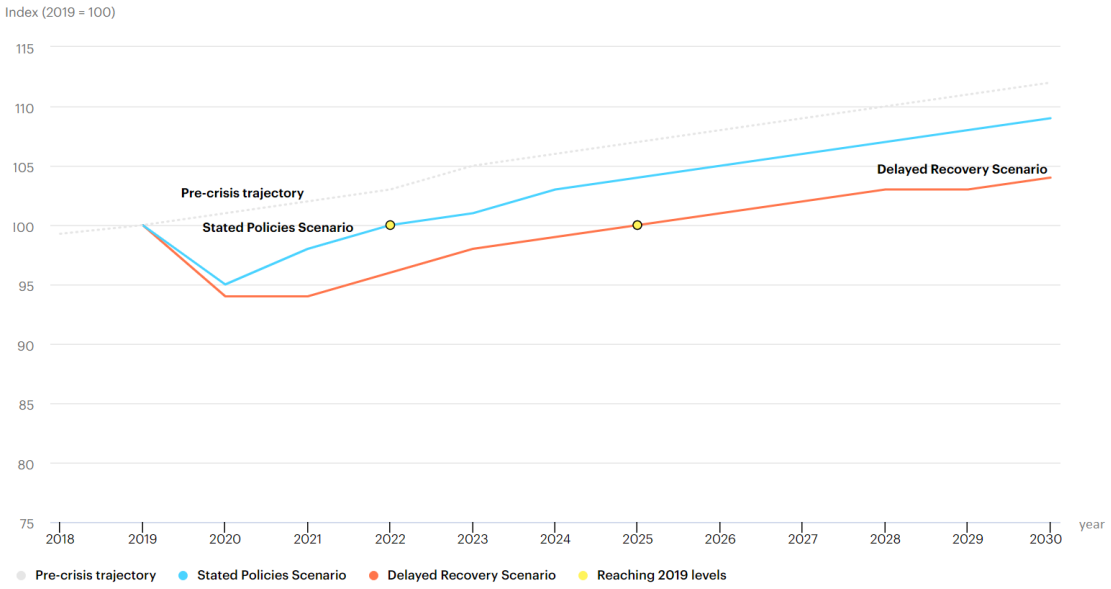

Figure 1.1: Predicted energy demand from year 2018 up to 2030 with year 2019 as a reference index at 100 [1]

The main energy sources used today are emitting a lot of CO_2 which is causing the world to heat up and subsequently causing more extreme weather, destroying biodiversity and changing the weather patterns. The use of fossil fuels, such as natural gas, oil and coal, are major contributors to these emissions. To reduce emissions and limit global warming, the Paris Agreement was agreed upon by several nations. One of the main goals of the agreement is to limit the earth temperature increase by reducing emission. Following the agreement, several nations have decided to invest more in renewable energy sources such as solar energy, wind energy, hydropower and biofuels, and carbon capture technology.

Renewable energy sources have the advantage of replenishing at a higher rate than they are consumed and have net zero CO_2 emissions. Figure 1.2 shows two graphs illustrating the totally energy supply by type of energy source and the total energy consumption in 1971 and 2019. From Graph 1.2a it can be observed that the total

percentage of fossil fuels has gone down as renewable energy sources have increased. However, because the total energy consumption has increased, the amount of fossil fuels consumed have increased as shown in Figure 1.2b, and are predicted to keep increasing [1].

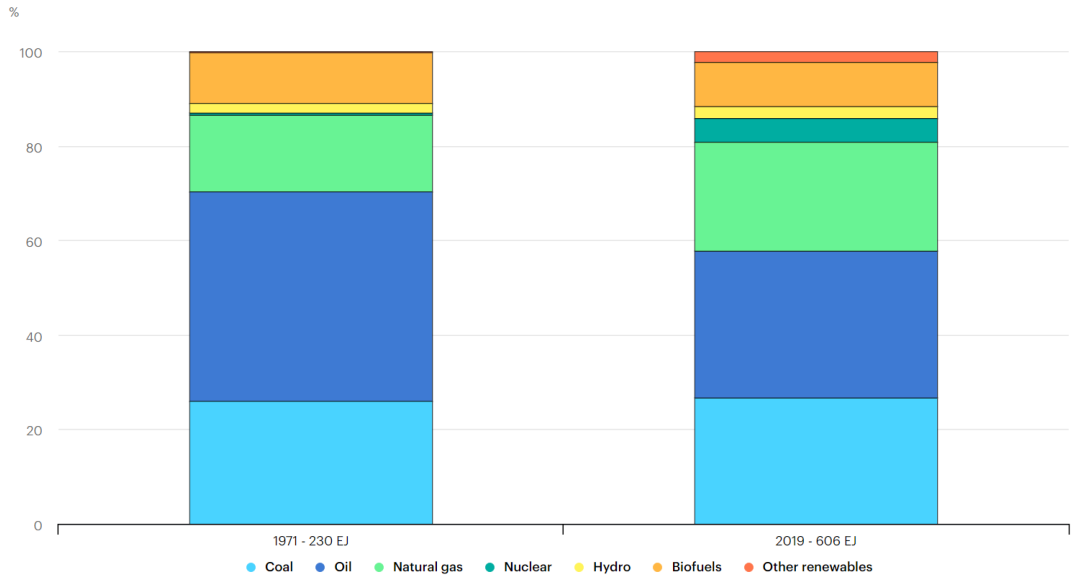

(a) Total primary energy supply by fuel in percentage for year 1971 and 2019.

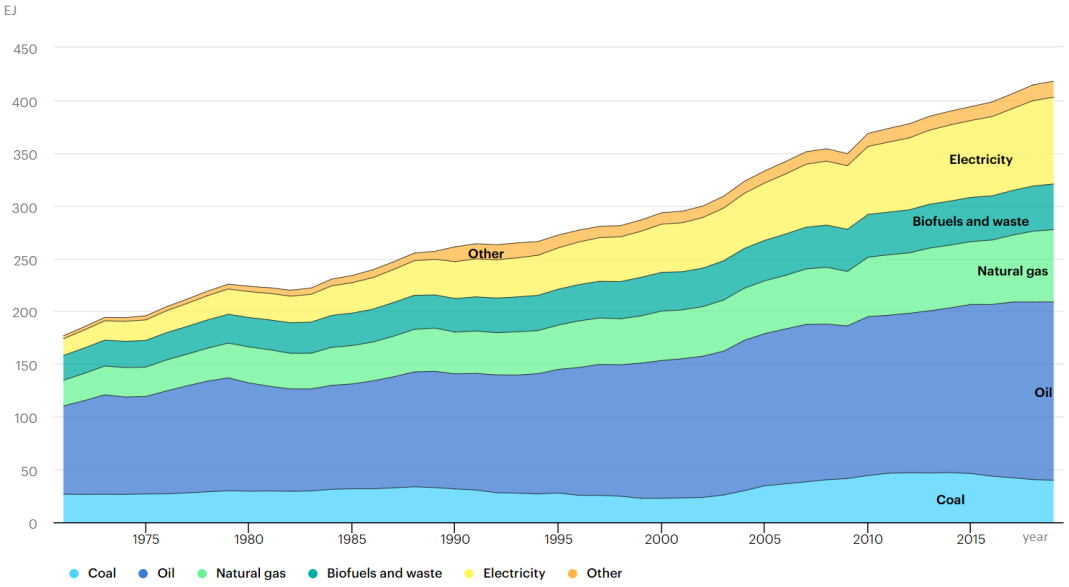

(b) Total world energy consumption in EJ from year 1971 to 2019 by energy source

Figure 1.2: Energy supply and consumption in 1971 and/up to 2019 [2, 3]

1.1 Biogas as a renewable energy source

As mentioned above, biogas is classified as a renewable energy source and can both contribute to satisfying the increasing energy demand and reduce CO_2 emissions.

According to the IEA, biogas and biomethane are the fastest growing forms of bioenergy but still require supportive policies to unlock their full potential [4]. In 2022 the European Commission presented the REPowerEU plan as a response to the disruption in the energy market caused by Russia's invasion of Ukraine in 2022. The plan includes a separate section, the bio-methane action plan, presenting actions to increase biogas and bio-methane production, and consequently reduce the dependency on Russian fossil fuels [5]. Because of increasing interests in biofuels more research and knowledge on the subject is needed and will contribute to development of biofuel production and infrastructure.

1.1.1 Composition and contaminants in biogas

The main components of biogas are methane (CH_4) and CO_2. The remaining compounds are impurities such as hydrogen sulphide (H_2S), water (H_2O), nitrogen (N_2) and other trace compounds. These compounds are important to remove not only to ensure high heating value,but also to ensure health and safety and to protect process equipment. Table 1.1 shows the different compositions of biogas based on the type of production pathway and the typical composition of natural gas (NG) from the North sea [6]. Natural gas has typically less CO_2 and trace contaminants than biogas and therefore treatment of the gas types differs.

Following in this section explanation of the contaminants CO_2, H_2O and H_2S will be presented, whilst other trace compounds will not be further considered.

Table 1.1: Composition of biogas from different production pathways and natural gas from the North sea [6]

Component	unit	Biogas plant	Sewage plant	Landfill	Natural gas
CH4	vol-%	60-70	55-65	45-55	87
CO_2	vol-%	30-40	35-45	30-40	1.2
N_2	vol-%	<1	<1	5-15	0.3
H_2S	ppm	10-20 000	10-40	50-300	1.5
C_2+	vol-%	-	-	-	12

Being the second most abundant compound in biogas, CO_2 varies between 15-60% [7]. CO_2 works as a dilutent and decreases the Wobbe index (WI) of the gas. The Wobbe index is defined as heating value divided by the square root of the specific density of the gas, as shown in Equation 1.1.

$$\mathrm{WI} = \frac{\Delta H}{\sqrt{\frac{\rho_{\mathrm{fuel}}}{\rho_{\mathrm{air}}}}} \qquad \left[\frac{\mathrm{MJ}}{\mathrm{m}^3}\right] \tag{1.1}$$

The WI is a parameter specified to ensure constant heat flow because of the varying composition in gases. Natural gas often has a lower fraction of CO_2 and thus a higher Wobbe index. The lower Wobbe index of natural gas is around 39.9 MJ/m^3 whilst for biogas with 38% CO_2 and 60% CH_4 it is 19.5 MJ/m^3 [8]. Therefore if biogas is to be put on the natural gas grid, the WI must be increased, hence CO_2 must be removed. CO_2 in itself is not harmful to process equipment but can react with other compounds present in the gas to create harmful acids.

Water is another common impurity and exists in the raw biogas as saturated water. Biogas at 35℃ contains approximately 5% water [7]. A complication of water in the biogas is that it can solidify into ice and cause damage to process equipment. Another problem is the reactivity of water with H_2S and CO_2 at high concentrations to form corrosive acids [9]. Various biogas utilisation systems have different water vapour tolerances. Water is normally not an issue in Combined heat and power (CHP) engines but problematic in gas grid injection or vehicle fuel applications . The most common technologies for water removal are absorption and adsorption. [7]

H_2S is always present in raw biogas and is formed by anaerobic digestion of proteins containing sulphur. The concentration of H_2S in biogas can vary greatly, but normal concentrations are between 80 and 4 000 ppm, depending on the biomass feedstock [10]. In cases where the feedstock contains high amounts of sulphur the concentration can be higher. For example, in the production of biogas from vinasse the concentration of H_2S is around 1% and up to 3% because of high content of sulphate [11].

Table 1.2: Symptoms and effects of H_2S concentrations to human health [12]

Concentration (ppm)	**Symptoms/Effects**
0.00011-0.00033	Typical background concentrations
0.01-1.5	Odour threshold (when rotten egg smell is first noticeable to some). Odour becomes more offensive at 3-5 ppm. Above 30 ppm, odour described as sweet or sickeningly sweet.
2-5	Prolonged exposure may cause nausea, tearing of the eyes, headaches or loss of sleep. Airway problems (bronchial constriction) in some asthma patients.
20	Possible fatigue, loss of appetite, headache, irritability, poor memory, dizziness
50-100	Slight conjunctivitis ("gas eye") and respiratory tract irritation after 1 hour. May cause digestive upset and loss of appetite
100	Coughing, eye irritation, loss of smell after 2-15 minutes (olfactory fatigue). Altered breathing, drowsiness after 15-30 minutes. Throat irritation after 1 hour. Gradual increase in severity of symptoms over several hours. Death may occur after 48 hours.
100-150	Loss of smell (olfactory fatigue or paralysis).
200-300	Marked conjunctivitis and respiratory tract irritation after 1 hour. Pulmonary oedema may occur from prolonged exposure.
500-700	Staggering, collapse in 5 minutes. Serious damage to the eyes in 30 minutes. Death after 30-60 minutes.
700-1 000	Rapid unconsciousness, "knockdown" or immediate collapse within 1 to 2 breaths, breathing stops, death within minutes.
1 000-2 000	Nearly instant death

The requirements to remove H_2S have many reasons. Table 1.2 shows the health effects of short-term exposure to H_2S for different concentrations. The effects of H_2S in human health are noticed at only few ppm for short time exposure. At 1 000 ppm H_2S the effect is nearly instant death. Thus, removal of H_2S is extremely important for health and safety issues. Furthermore, H_2S can cause environmental damage, e.g. acid rain, or lead to formation of SO_2 that is a long-range pollutant. Not only is H_2S dangerous for people and the environment, it is also corrosive to process equipment. Sulphur stress cracking (SSC) is the most common corrosive mechanism between metal equipment and H_2S and can occur from 50 ppm H_2S [13]. Consequently removing H_2S is not only important for human health and the environment but also to ensure well working process equipment.

1.1.2 Production and utilisation

Two of the most common biogas production pathways are anaerobic digestion (AD) and gas collection from landfills. As AD is a more controlled process, it generally produces a higher energy content gas. On the other hand, landfill-biogas is cheaper but contains many extra contaminants [6]. The AD production pathway for biogas and biomethane is illustrated in the Figure 1.3.

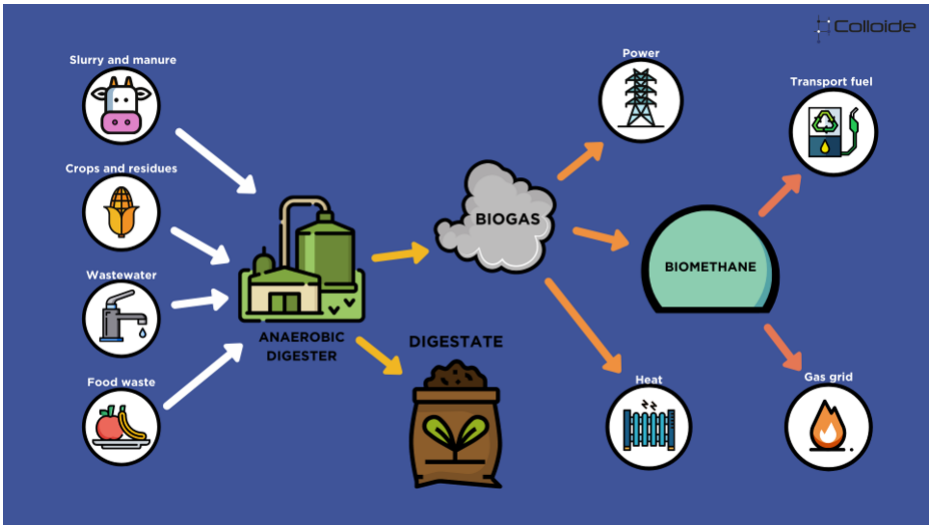

Figure 1.3: Production pathway for biogas and biomethane [14]

First feedstock is fed to an anaerobic digester where the organic matter is broken down in the absence of oxygen. From the digester the products are the digestate, that can be turned into fertiliser, and biogas. Based on the source of feedstock the biogas can have a wide variety of composition, as shown in Section 1.1.1. Depending on the composition and intended utilisation, further conditioning (removal of trace

contaminants, e.g. H_2S) and/or upgrading (removal of CO_2) would be needed to meet the emission and healthy standards in the given country for given application.

There is increasing interest in production of biogas from vinasse, a bi-product in the production of bioethanol from sugarcane. Bioethanol production is increasing around the world, especially in South America and Asia, however suffers from pollution and greenhouse gases (GHG) emissions, partially due to poor handling of the vinasse [15]. Vinasse has a great potential for biogas production due to its high organic content: it contains about 11% of the original energy from the sugarcane juice [16]. Furthermore, AD of vinasse decreases pollution and GHG emissions. Biogas produced from vinasse typically has a high concentration of H_2S, up to 3%, and requires desulphurisation before usage [17]. Typically, biogas that is made from vinasse has been used to produce electricity (less strict requirements), however there is an increasing interest to focus on production of biomethane as a substitute for NG or vehicle fuel.

Biogas has typically been used for production of electrical power in internal combustion engines (ICE) [7]. In this utilisation only more aggressive contaminants, e.g. H_2S, must removed while a high amount of CO_2 can remain. Production of bio-methane has an increasing interest as it can be injected into the NG gird network, fully or partially substituting natural gas. However, NG grid specification are stricter than CHP equipment specification and need both upgrading and conditioning before it can be put on the distribution network. Table 1.3 shows some typical gas specifications for CHP engines and NG standards in Germany and Sweden. The different areas have different specifications, e.g. in natural gas the amount of H_2S is

Table 1.3: Specification for CHP engines and natural gas grid [7]

CHP equipment specification		
Values	ICE w/o catalyst	Sterling engines
Calorific value range [MJ/Nm^3]	14.9-44.7	medium: 11.9-21.9 high: 85.7
Sulfur [ppmv]	542-1742	2 800
Moisture	pressurised dew point -6.7℃ less than the gas temperature	pressurised dew point -6.7℃ less than the gas temperature
Natural gas grid specifcation per country		
Values	Germany	Sweden
lower WI [MJ/Nm^3]	lower: 37.8-46.8 higher: 46.1-56.5	43.9-47.3
CH4 [%]	-	97 ± 2
CO_2 [%]	<6	<3
H_2S [mg/m^3]	<5	<15.2

specified while for CHP equipment total sulphur content is specified. What can be compared is the calorific value range with the WI. Typically ICE equipment have lower calorific value than natural gas.

1.2 Technologies for CO_2 capture

There are typically three main ways to capture CO_2: pre-combustion, post-combustion and oxy-combustion. In pre-combustion the fuel is reacted with air and steam to create CO_2 and H_2. The CO_2 is removed before the combustion is complete. Oxy-combustion is similar to pre-combustion but uses pure oxygen which gives a product of nearly pure CO_2 and water. In post-combustion CO_2 is captured after the fuel has been burned. This can be done in many different ways, e.g. absorption, adsorption, distillation, membranes or other technologies. H_2S and CO_2 are two of the most common gas phase impurities and in most cases they are removed in different stages by different technologies, but they can also be co-removed. The removal process of these impurities can be grouped in seven types of processes as shown in Figure 1.4 [18]. The processes that are applicable for both compounds are: chemical or physical absorption, membrane separation and adsorption.

Table 1-2
Guidelines for Selection of H_2S and CO_2 Removal Processes

Type of Process	Acid Gas H_2S	Acid Gas CO_2	Plant Size	Partial Pressure	Sulfur Capacity
Absorption in Alkaline Solution	A	A	H	L	H
Physical Absorption	A	A	H	H	H
Absorption/Oxidation	A	—	H	L	L
Dry Sorption/Reaction	A	—	L	L	L
Membrane Permeation	A	A	L	H	L
Adsorption	A	A	L	L	L
Methanation	—	A	L	L	—

Notes: A = Applicable, H = High, L = Low; dividing line between high and low is roughly 20 MMscfd for plant size, 100 psia for partial pressure, and 10 tons/day for sulfur capacity.

Figure 1.4: Removal processes for H_2S and CO_2 [18]

Physical absorption is driven by the H_2S or CO_2 partial pressure difference of the gas phase and liquid phase. One of the main advantages of physical absorption is the cheap solvent used, e.g. water, however the process is not economical competitive for gases with low partial pressure. Therefore, physical absorption is typically used for acid gas removal from high pressure natural gas [19].

Membrane permeation uses membranes as a selective barrier to separate the gas molecules and is based on the rate of permeation. Membranes have many advantages

such as: low capital investment, easy to operate and scale up, and low environmental impact. Some disadvantages of membranes are that they can only do bulk removal of acid gases, they become quite costly when up scaling, and particle cleaning of the gas is essential [20].

Adsorption processes are good for removal of low concentrations of H_2S and are a typical technology for removal of H_2S from biogas. However for removal of CO_2 the gas needs to have a high CO_2 partial pressure to be preferred technology [21] The most common adsorption technique for CO_2 removal is Pressure swing adsorption (PSA), which can also be used for H_2S.

1.3 Chemical absorption for acid gas removal

Chemical absorption works in a similar way to physical absorption, but instead of water it uses a chemical compound, e.g. alkonolamines or alkalinesalt solutions, and benefits from both physical absorption and chemical reaction between the solvent and the acid gas.

An illustration of chemical scrubbing for CO_2 is shown in Figure 1.5 . An absorption column is used to facilitate the mass transfer of acid gas (CO_2 and H_2S) from gas to liquid phase. From the absorption column the CO_2- and H_2S-free gas, sweet gas, leaves at the top, and the rich solvent at the bottom. This liquid is heated up and sent to a stripper column to regenerate the solvent and release the acid gas that is removed at the top of the column.

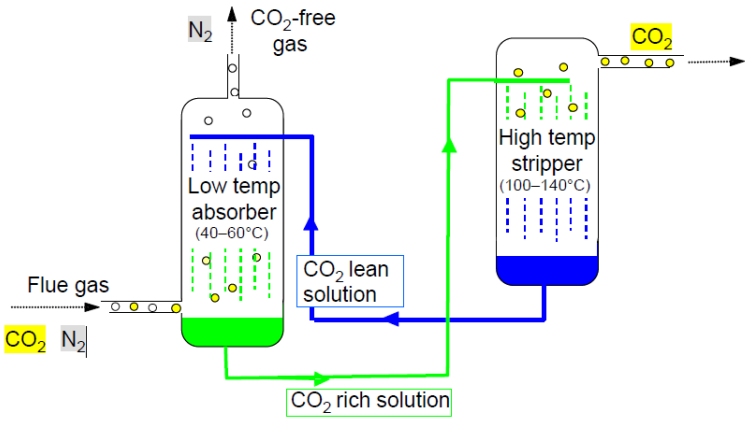

Figure 1.5: An illustration of chemical scrubbing for CO_2 removal [22]

The absorption and stripper column work in a temperature swing process. A cold solvent solution has a higher affinity to the acid gases, thus to increase the absorption, typically, the absorption column works at 40-60°C. The stripper, on the other

hand, needs to reverse the chemical equilibira, and higher temperature is used to release the acid gas. The stripper typically works at 100-140℃ [22]. Not only is the temperature important but also the partial pressure of the acid gases in the stream. The solubility of acid gas in the solution is proportional to its partial pressure. Therefore, it is necessary to have high partial pressure in the inlet gas stream to the absorber and low partial pressure in the outlet gas stream from the stripper.

Driving the regeneration in the stripper column is the reboiler at the bottom of the column. The reboiler provides: (i) heat for evaporating part of the solvent (mainly water) diluting the acid gas and creating a driving force inside the stripper column, (ii) the required energy to reverse the absorption reactions, and (iii) the energy to rise the temperature of the solvent in the column [22]. The reboiler is the main energy consumer and therefore optimisation of the reboiler duty is important to reduce the cost of the removal. Approximately 70% of operating costs of a gas sweetening plant, excluding labour expenses, are due to the energy required for the regeneration of the solvent [23]. To reduce sensible heat loss the solvent should have high cyclic capacity (CC), which is defined as:

$$\mathrm{CC} = \alpha_{\mathrm{rich}} - \alpha_{\mathrm{lean}} \tag{1.2}$$

where α is the loading in mol acid gas/mol solvent [24].

Another important part of the chemical absorption is the circulating liquid flow rate. Higher flow rates are desired to increase the liquid residence time, and thus the acid gas absorption. However, increasing the circulating flow rate will increase the energy consumption in the reboiler duty as well as corrosion rate and acceleration of amine degradation. Furthermore, the capital expenditure (CAPEX) of the process will increase because the liquid flow rate affects the size of facilities such as absorber, piping, and stripper [23]. A high concentration of amines in the circulating liquid is also desired to increase contact between acid gas and amine, and thus the absorption rate. However high concentrations of amine increase the reboiler duty and corrosion, just as increasing flow rate and risk precipitation do.

1.3.1 Amine solvents in chemical absorption

Amine absorption processes have traditionally not been used for biogas conditioning because they have not been economically feasible for low-flow and low-pressure applications [10]. However, biogas is gaining an increasing interest as an energy source and new feedstock to produce biogas, such as vinasse from bioethanol production, poses new challenges to commonly used H_2S removal technologies as it produces a

biogas with high H_2S content. In this context, amine absorption technology rises as a potential candidate as it also has the advantages of low CH_4 losses, low electricity demand and high CH_4 content efficiency.

Amines have a hydroxide group that favours solubility in water, and an amino group that promotes a reaction with the acid gas. Amines are divided into four groups: primary, secondary, hindered and tertiary amines. Typically, increasing the amine side group gives lower heat of reaction and slower kinetics [25]. One of the most studied amines is the primary amine monoethanolamine (MEA), and is often taken as the benchmark technology for CO_2 capture application [26]. MEA, 2- amino-2-methyl-1-propanol (AMP) and piperazine (PZ) are shown in Figure 1.6. MEA has the advantage of being well researched and explored, and its properties are well known. MEA is often the preferred solvent for gas streams containing low concentrations of CO_2 and H_2S, and has the advantage of being cheap. Nevertheless, MEA is rapidly being replaced by other solvents because of its disadvantages such as low loading capacity (0.5 mol CO_2/1 mol MEA), high corrosiveness and the high energy requirement for regeneration. [25–27]

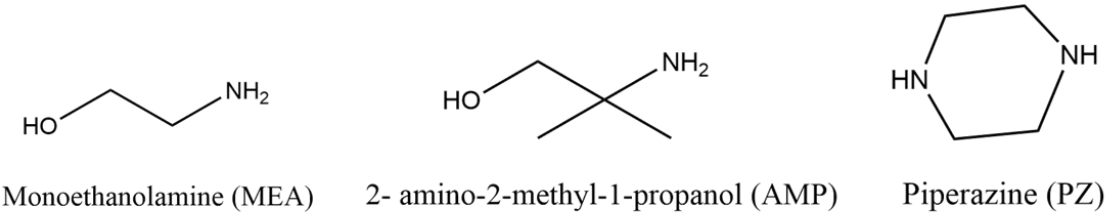

Figure 1.6: Molecular structures of monoethanolamine (MEA), 2- amino-2-methyl-1-propanol (AMP) and piperazine (PZ)

Other amines that have been studied are AMP and PZ. AMP is a primary sterically hindered amine; it is a MEA with the alpha carbon filled with CH_3-groups. This sterical hindrance lowers the carbamate stability and makes the behaviour more similar to tertiary amines. AMP is expected to have higher cyclic capacity but suffers from low absorption rate being slower than MEA [28]. PZ is a cyclic secondary amine with two amine groups in molecule. It has a higher absorption rate, 2.6 times faster than MEA [29]. Furthermore, it is more stable at higher temperatures and has lower volatility than MEA . However, studies have shown that PZ has bad solvent solubility and can suffer from precipitation [29, 30].

A blend of AMP and PZ has been looked into and is named CESAR-1 solvent. The AMP/PZ blend is shown to improve the CO_2 recovery and reduce the reboiler duty for solvent regeneration [31, 32]. AMP/PZ blends often have higher concentration of AMP than PZ and uses PZ as a promoter. Though AMP has a slow absorption rate,

because of the sterical hindrance, it still has a competitive protonation constant. As AMP has a higher concentration, it will accept more protons over PZ, thus allowing the non-protonated PZ to enhance mass transfer of CO_2, as shown in Equation 1.6 [22, 33]. Brúder et al. [34] found that 40 wt% CESAR-1 solvent was the highest concentration which did not form solid precipitates during the absorption of CO2 at 40 °C (but what AMP/PZ ratio?)

There are two ways amines contribute to acid gas absorption. The first is indirectly where the amine dissociates and makes hydroxide-ions, as shown in equation 1.3. The OH^--ions increase the alkalinity of the solution and drives the dissociation of CO_2 and H_2S as shown in equations 1.4 and 1.5. These reactions bind the acid gas as bicarbonate and bisulphide ions into the liquid phase. Both ions can further dissociate into carbonate and sulphide ions, but these rate constants are much smaller. The alkalinity of the solution drives these equations and is especially important for H_2S absorption as many applications of biogas or biomethane require low concentrations of H_2S. The dissociation of H_2S in water as a function of pH is illustrated in Figure 1.7. The figure shows that the pH has to be higher than 9 for H_2S to fully dissociate into ions.

$$H_2O + RR'NH \rightleftharpoons RR'NH_2^+ + OH^- \tag{1.3}$$

$$H_2O + CO_2 \rightleftharpoons H^+ + HCO_3^- \tag{1.4}$$

$$H_2S \rightleftharpoons H^+ + HS^- \tag{1.5}$$

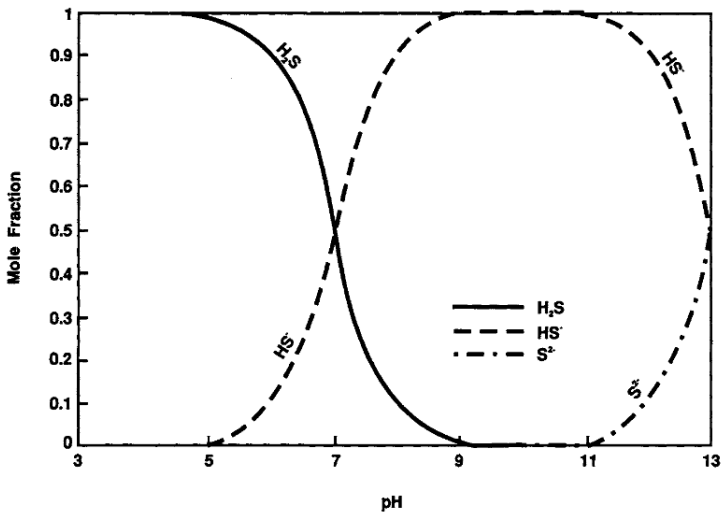

Figure 1.7: H_2S and its dissociated ions distribution as a function of pH [35]

The second way of acid gas absorption is direct reaction between amine and the acid gas. For CO_2 the mechanism is different for primary/secondary amines and tertiary amines, whilst for H_2S the reaction is independent of the class. Primary and secondary amines react directly with CO_2 as shown in equation 1.6. This reaction is very fast, and will dominate over equation 1.4 at high concentrations of amine. However two amine are needed per one CO_2 molecule. Therefore though the reaction gives high absorption rate more solvent is needed.

$$2\,\mathrm{RR'NH} + \mathrm{CO_2} \rightleftharpoons \mathrm{RR'NCOO^-} + \mathrm{RR'NH_2^+} \tag{1.6}$$

For tertiary and hindered amines the overall reaction occurring for CO_2 is shown in equation 1.7, where CO_2 first reacts with water to form bicarbonate, which then combines with the amine. This reaction is slower than equation 1.6, but only needs one amine per CO_2 molecule. Therefore tertiary and sterically hindered amines are often used with promoters as explained for the CESAR-1 solvent.

$$\mathrm{R_3N} + \mathrm{H_2O} + \mathrm{CO_2} \rightleftharpoons \mathrm{HCO_3^-} + \mathrm{R_3NH^+} \tag{1.7}$$

The direct reaction between H_2S and amines is shown in 1.8. This reaction is no different from the dissociation of H_2S in water only here the amine is the corresponding base. Because the amine itself is a base, and thus increases the pH, having enough amine in the solution is important to drive the dissociation with both amine and water.

$$\mathrm{H_2S} + \mathrm{RR'NCH_3} \rightleftharpoons \mathrm{RR'NCH_4^+} + \mathrm{HS^-} \tag{1.8}$$

1.3.2 Amino acid salts solvents in chemical absorption

Amino acid salts (AAS) are proposed as an alternative for alkonol amines used in absorption technology. AAS are reported to have lower volatility, higher CO_2 capacity and lower regeneration energy than amines. Furthermore, the natural occurrence of AAS makes them low toxic, environmentally friendly and have higher stability towards oxidative degradation [36–40].

One of the first processes that used amino acid salts, sodium alanine and diethyl- or dimethylglycine, was the Alkazid process by BASF. However, this process is no longer competitive. Other processes such as the Giammarco-Vetrocoke process uses

a glycine activator, but the main solvent is highly toxic asenite [41]. In 2009 Siemens started working on the POSTCAP project using amino acid salts for CO_2 capture [42].

Amino acids are characterised by their acid and amine group on either side of the molecule, the simplest amino acid is glycine and is shown in the Figure 1.8. The amine group can be protonated and the acid group can be de-protonated and is therefore a zwitterion that can have both negative and positive charge at the same time.

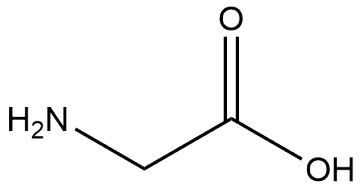

Figure 1.8: Molecular structure of glycine

The charge of the ion is determined by the pH in the solution. At low pH the ion will be in its protonated form while at high pH it will be deprotonated. The solubility of the amino acid depends on both temperature and pH. The solubility of AAS increases for high and low pH as this is when the AAS is in its protonated or deprotonated state as shown in Figure 1.9.

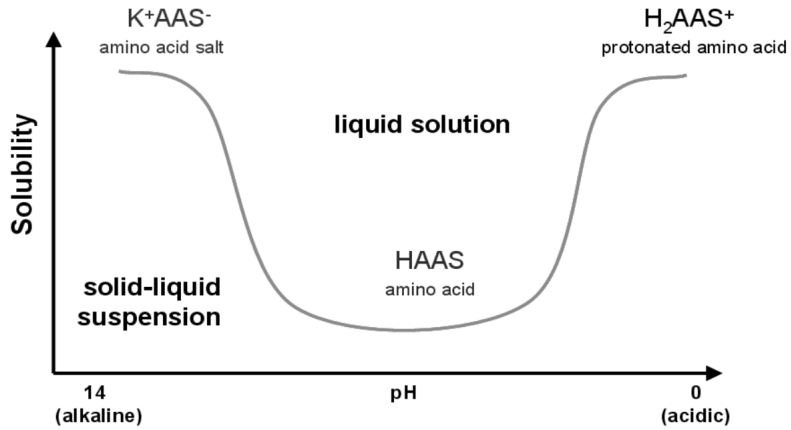

Figure 1.9: Solubility of amino acid as a function of pH [43]

In its deprotonted state the amino acid can react with CO_2 as shown in the following equation:

$$CO_2 + 2\,NH_2{-}R{-}COO^- \rightleftharpoons COO^-{-}R{-}NHCOO^- + COO^-{-}R{-}NH_3^+ \qquad (1.9)$$

It is therefore important that the amino acid is deprotonated. This can be done by mixing a base with the amino acid to form an amino acid salt, as shown in the following equation where sodium hydroxide (NaOH) reacts with glycine in its zwitterion form to form sodium glycinate (SG):

$$NaOH + {}^{-}COO{-}CH_2{-}NH_3^{+} \longrightarrow Na^{+}OOC{-}CH_2{-}NH_2 + H_2O \tag{1.10}$$

Amino acid salts are known for precipitating when reacting with CO_2 and many processes use this as an advantage. When AASs precipitate more carbamate is formed and thus increasing the CO_2 absorption capacity of the solvent[44]. Precipitation is dependent on the concentration of AASs in the solvent and temperature. The DECAB+ is similar to chemical absorption process but have a solid-liquid separator for slurry handling after the absorption column. The SL-separator is used for slurry handling of the precipitation and it can lower the reboiler duty, but have the disadvantages of slurry handling and crystallisation control [45].

2 Motivation for the project

The objective of this work is to study the use of the amino acid salts SG and the amine blend CESAR-1, a more traditional solvent, for co-absorption of H_2S and CO_2 from biogas to make bio-methane at natural gas grid standards. The objective has been divided into the following sub-tasks:

- Explore the use of amino acid salts in chemical absorption to treat biogas with CO_2 and high H_2S concentrations
- Investigate the precipitation of SG with absorbing CO_2
- Study the use of CESAR-1 solvent for co-absorption of CO_2 and H_2S from biogas
- Preform a profitability analysis of the chemical absorption process with the CESAR-1 solvent

3 Material and Method

This section describes the method of the thesis. The chronological order of the thesis was simulation with SG solvent, laboratory work followed by simulation with CESAR-1 solvent and ended with analysis and comparison of the data. In this section the simulation parts will be explained together, thereafter the laboratory procedure.

3.1 Setting up the simulation

All simulations in this report were carried out in Protreat version 7.0- *Rate-based Gas Treating Simulator* by Optimised Gas Treating, Inc..The program uses the Deshmukh-Mather thermo package and considers the reactions given in Table 3.1. The Deshmukh-Mather model is based on the extended Debye-Huckle theory on dilute electrolytes, and calculates the excess Gibbs free energy based on activity coefficients [46].

Table 3.1: Reactions considered in the Deshmukh-Mather model [46]

Reactions considered in the Deshmukh-Mather model	
$H_2O \rightleftharpoons H^+ + OH^-$	Ionization of water
$H_2S \rightleftharpoons H^+ + HS^-$	Dissociation of hydrogen sulfide
$H_2O + CO_2 \rightleftharpoons H^+ + HCO_3^-$	Dissociation of carbon dioxide
$H_2O + RR'NH \rightleftharpoons RR'NH_2^+ + OH^-$	Dissociation of alkanolamine
$RR'NH + CO_2 \rightleftharpoons RR'NCOO^- + H^+$	Formation of carbamate
$HS^- \rightleftharpoons H^+ + S^-$	Dissociation of bisulfie ion
$HCO_3^- \rightleftharpoons H^+ + CO_3^-$	Dissociation of bicarbonate ion

The removal of H_2S and CO_2 from biogas was simulated in a chemical absorption plant as shown in Figure 3.1. The inlet biogas had a flow of 100 kmol/h at 1 bara and 35℃ with a composition of 57% methane, 40% CO_2, 3% H_2S in mol% and saturated with water. This composition was used to simulate a biogas with high H_2S concentration, typically found for biogas production from vinasse. A compressor, cooler and flash tank were added before the absorber column to make sure the inlet stream to the absorber was at 35℃ and had a vapour fraction equal to one. This was done to ensure fixed pressure inlet conditions to the absorber if the composition or properties of the biogas changes. The absorber and stripper column specifications are presented in Table 3.2.

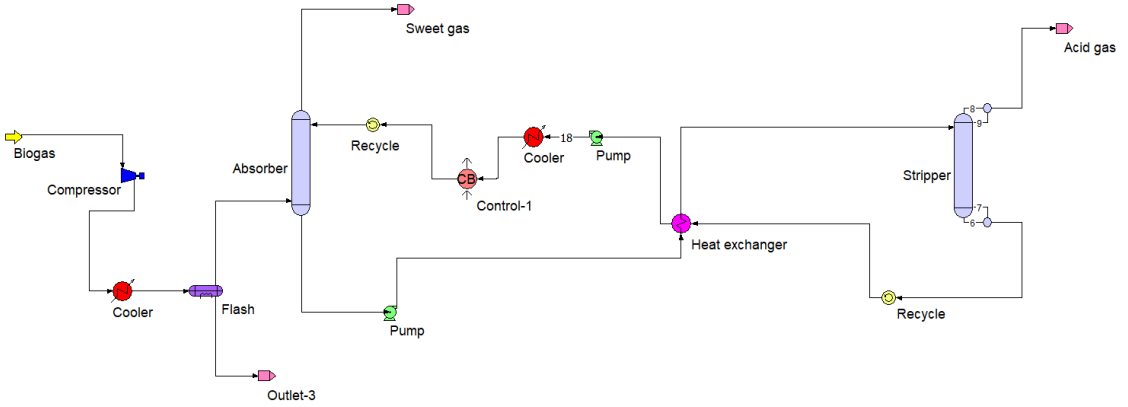

Figure 3.1: Simplified process scheme of the amine scrubbing simulation in Protreat.

Table 3.2: Absorber and stripper column specifications used in the simulation

Object	**Value: Absorber/Stripper**
Flooding [%]	70
Packing size	M350.X
Packing depth [m]	3, 6, 8, 10, 15, 20 or 30
Packing type	MELLAPAK

To fully specify the system a minimum temperature approach at 5°C was used in the heat exchanger. The loading of the system was defined as:

$$\alpha = \frac{[\text{mol acid gas}]}{[\text{mol solvent}]} \tag{3.1}$$

where acid gas is H_2S, CO_2 or a combination of both. The specific reboiler duty (SRD) was defined as:

$$\text{SRD} = \frac{\text{Reboiler duty [MW]}}{\text{mass flowrate [kg/s]}} \tag{3.2}$$

and the liquid-gas (L/G) ratio was defined as lean liquid entering the absorber over gas entering the absorber, in units mol liquid/ mol solvent.

The solvents used in the simulations were 45 wt% SG and 40 wt% CESAR-1 (27/13 wt% AMP/PZ) during the simulation. The goal of the simulations was to reduce the impurities in the biogas to meet the natural gas grid standards of 1 mol% CO_2 and 3.578 ppm H_2S. These values are used as they are typical standards used by countries in the EU [7].

The solver function in Protreat was used to adjust the flow rate of the system to reach the target value in the sweet gas. As the solver block can only target on component at the time, simulations meeting the 1 mol% CO_2 were preformed,

thereafter a specification of 3.578 ppm (5 mg/m^3) H_2S. Limiting H_2S to 3.578 ppm subsequently limits CO_2 as this is a tighter specification.

3.1.1 SG simulations

Firstly a base case with 20 metre absorption and stripper columns with a specification of CO_2 concentration at 1 mol% was conducted to find the optimum L/G-ratio for lowest energy consumption. Afterwards, the column heights were changed to 30, 15, 10, 8 and 6 metres to see how the reboiler duty changed for column height followed by specifying the H_2S concentration to reach the NG grid requirement. The base case was followed by an optimisation where the H_2S inlet concentration was changed to 2, 1, 0.1 and 0.01 mol% for the 20 metre column to reach the NG grid requirement. The simulations with the reduced inlet H_2S concentration were preformed to include biogas made from other sources than vinasse containing less H_2S.

Secondly simulations with an inter-cooler (IC) in the absorber column were done. 20 metre absorber and stripper columns were used with IC ranging from 4 to 1 metre from the top to see how the temperature profile in the absorber column changed. The part of the PFD that differs from the main PFD shown earlier is in Figure 3.2. The outlet temperature of the cooler was set to 25°C.

3.1.2 CESAR-1 simulations

CESAR-1 simulations were similar to those with SG; a base case with 20 metre absorption and stripper columns with a specification of CO_2 concentration at 1 mol% was conducted to find the optimum L/G-ratio for lowest energy consumption. Secondly, the column heights were changed to 30, 15, 10, 8 and 6 metres to see how the reboiler duty changed for column height followed by specifying the H_2S concentration in the sweet gas to 3.57 ppm for all column heights. Lastly, simulations with H_2S inlet concentration of 2, 1, 0.1 and 0.01 mol% were preformed. First a base case for each inlet was done, then optimisation with change of column heights of 20, 15, 10, 6 and 3 metres was looked into.

3.2 Laboratory procedure

There were issues in accessing the laboratory in the early stages of the thesis, and it was therefore not until after the simulations with SG solvent that the laboratory

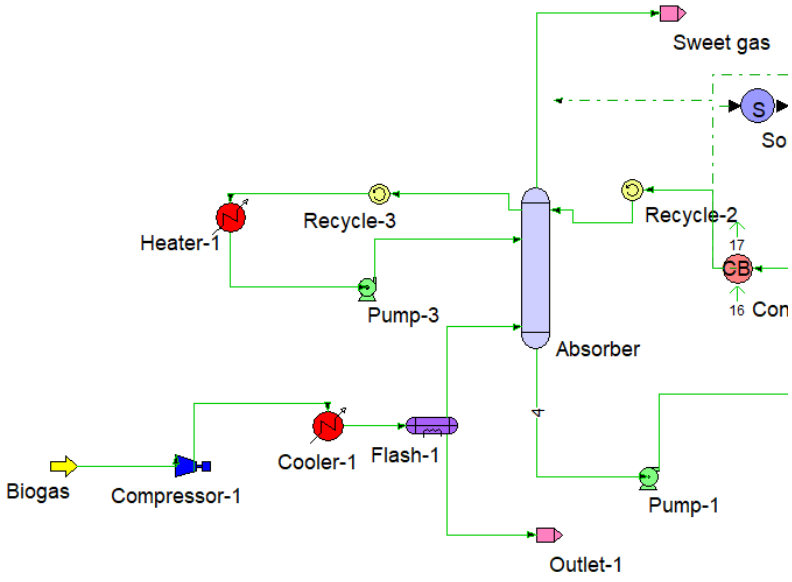

Figure 3.2: Simplified process scheme of the absorption column with one inter cooler.

experiment was conducted. The laboratory experiment was undertaken as more research on the topic had been conducted and there was a noticeable possibility of precipitation at the used weight percentage.

The solvent sodium glycinate, SG, was made by mixing equimolar glycine (purity > 98.5 %, Sigma-Aldrich) and sodium hydroxide (purity 98.8 %, VWR chemicals). Distilled water was added to make the desired solution concentration. Two parallels of 45 and 35 wt% was made. Pure carbon dioxide was used during the experiment.

To find the concentration where precipitation occurs, CO_2 was injected into the SG solution while the increase in weight was noted to calculate absorbed CO_2. A scheme of the setup is shown in Figure 3.3. Samples of the solution were taken for further analysis. The amount of CO_2 in the solutions was determined by inorganic carbon analyser TOC-L CPH/CPN analyser from Shimadzu. Approximately 400 µL of solution and 40 g of Millipore Ultrapure water was used in each sample.

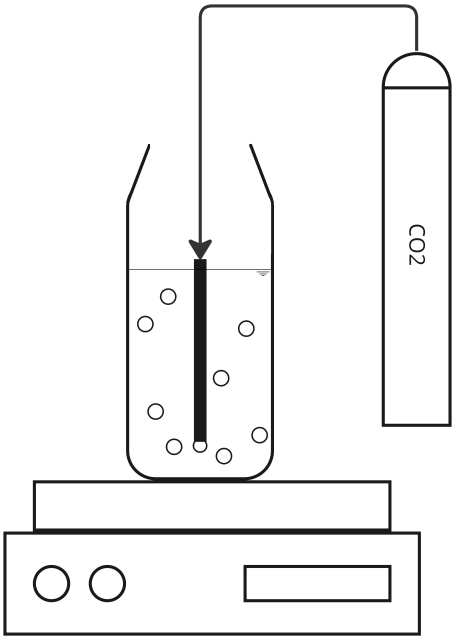

Figure 3.3: Simplified scheme of the laboratory setup

4 Laboratory results

To validate the simulation model, solubility experiments with CO_2 in sodium glycinate were preformed. The two experiments at 45 wt% showed precipitation after 2 minutes, and after 5 minutes the solution had turned to a thick mass. It was only possible to do TOC analysis of the solution before the solution turned thick. Pictures from before and after the experiment are shown in Figure 4.1.

(a) 45wt% SG solution before the experiment

(b) 45 wt% SG solution after 5 min of CO_2 injection

Figure 4.1: 45 wt% SG solution before and after experiment

The two experiments at 35 wt% did not show any precipitation during the experiment, however after letting the solution stand for 1 hour precipitation could be observed in the solution. After resting for 24 hours there was a clear distinction between solid and liquid phase. Both cases are shown in Figure 4.2 below. The parallels of 35 wt% were tested when the precipitation solubilised again by applying heat to the solutions. It was found that the solutions were clear at 80 °C.

There were two clear differences between the 45 and 35 wt% cases. Firstly the 45 wt% had precipitation after only a couple of minutes, while precipitation was not observed for the 35 wt% parallels. Secondly, while the 35 wt% parallels had a clear heterogeneous mixture with a solid-liquid interface after standing for 24 hours, the 45wt% parallels did not separate and stayed as a homogeneous mixture.

(a) 35 wt% SG solution, to left beaker just finished experiment and to right beaker 1 hour after experiment

(b) 35 wt% SG solution 24 hours after experiment

Figure 4.2: 35 wt% SG solution 1 hour and 24 hours after experiment.

Rabensteiner et al. [47] reported no problems of precipitation using 40 wt% SG in their pilot plant test facility. On the other hand, Aronu et al. [48] found precipitation for SG solutions of 5 and 6.8 M. The solutions were clear before absorption and afterwards they became a thick viscous solution and a white paste solution respectively. Both cases were insoluble or not dissolved at 80℃. The results after absorption are similar to the parallels of 45 wt% . Aronu et al. [48] also did an experiment with potassium glycinate (PG) solution of 5M. After absorption the solution settled into two phases, similar to the parallels of 35 wt%. It was further reported that the white precipitate disappeared at 80℃, once more similar to the 35 wt% parallels.

The CO_2 loading from weight measurements and from the TOC analyser over the course of time are shown in Figure 4.4 and 4.3.The average deviation between calculated CO_2 absorbed and the TOC analysis is shown in Table 4.1. It should be noted that TOC analyser could only calculate the loading from the solutions that were liquid. Therefore the calculated loadings have more data points.

Table 4.1: Average deviation between calculated and TOC analysed CO_2 absorption in each experiment/round.

Experiment	Average deviation[%]
1, 45 wt%	17.5
2, 45 wt%	7.6
1, 35 wt%	6.4
2, 35 wt%	16.8

The loadings are similar for the first five minutes, thereafter the TOC analyser was not able to analyse the 45 wt% parallels, but the 35 wt% parallels reach a loading of approximately 0.6 mol CO_2/ mol solvent. The calculated loadings show a wider spread after five minutes with the 45 wt% parallels reaching 0.7 mol CO_2/ mol solvent and the 35 wt% parallels avrages at 0.55 mol CO_2/ mol solvent. The TOC analyser is more precise in analysing amount of CO_2 in the solutions and it is therefore assumed that the deviations in the calculated loadings are due to human error. It was expected that the loadings would reach 0.5 mol CO_2/ mol solvent as this is the theoretical amount of CO_2 a primary amine can absorb. The increase to 0.6 CO_2/ mol solvent may be because of physical absorption, i.e. formation of bicarbonate, or precipitation occurring in the solution increasing the CO_2 absorption capacity.

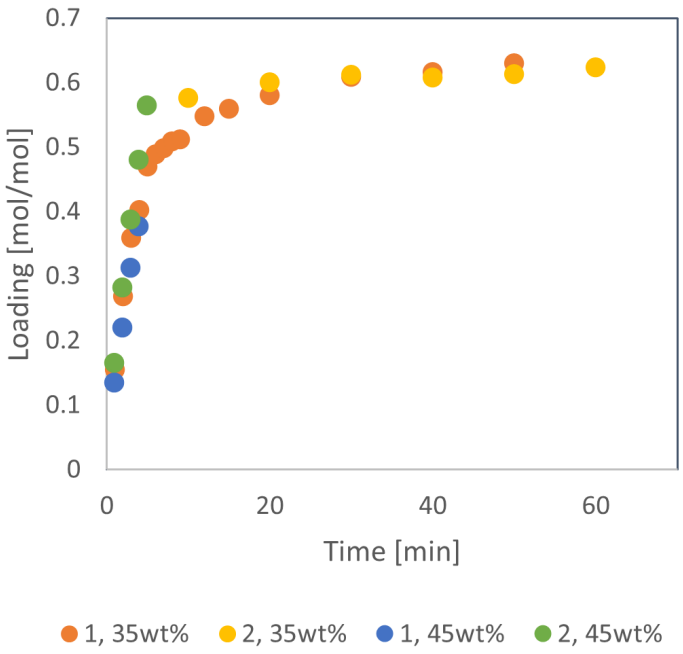

Figure 4.3: CO_2 loading over time from TOC analyser

Though it is clear from the results that SG can absorb CO_2 and in some cases reach a loading of 0.6, precipitation is evident for both parallels of 45 and 35wt%. It can therefore not be advised to use SG at these weight percentages for an liquid-gas absorption technology as chemical scrubbing. However it does fit in with other processes, like the DECAB+ process.

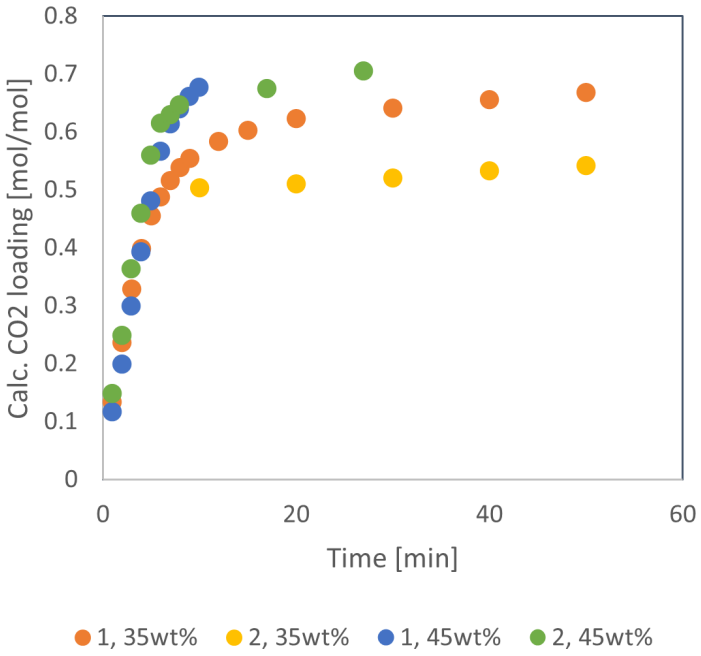

Figure 4.4: CO_2 loading over time from calculation based on weight of solution

5 Validation of simulation model

To validate the simulation model used in Protreat, vapour-liquid equilibrium (VLE) was simulated for SG with CO_2 and CESAR-1 with CO_2. The simulation consisted of a flash tank as illustrated in Figure 5.1. In the SG-CO_2 case the solvent inlet stream had a SG concentration of 1, 5, 10, 15, 20, 25, 30 wt%, while to CESAR-1-CO_2 case had AMP/PZ concentrations of 27 wt% AMP and 13 wt% PZ. The validation was only done between the solvents and CO_2, because of either non existing data for the solvent with H_2S or limited data for the given solvent composition.

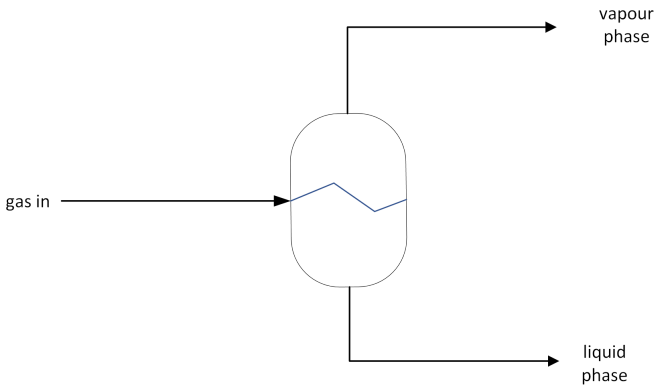

Figure 5.1: Simplified scheme of VLE simulation

To find the deviation between the simulation model and the literature value the following equation was used,

$$\chi_i = \frac{P^{lit} - P^{calc}}{P^{lit}} \times 100\% \tag{5.1}$$

Furthermore, the average deviation, AD was found for each system by the following equation,

$$AD = \frac{1}{n} \sum^{n} |\chi_i| \tag{5.2}$$

For the SG-CO_2 system only the results from the 10 wt% case will be shown here as the different weight percentages show a similar trend. Graphs with different weight percentages can be found in Appendix A. Figure 5.2 shows the partial pressure of CO_2 as a function of loading. The partial pressure is shown on a logarithmic scale. In the graph the lines represent the simulation model while the scatter plots represent the literature values. In general there is little consistence between the simulation and literature values. However there is also little consistency between the literature values themselves.

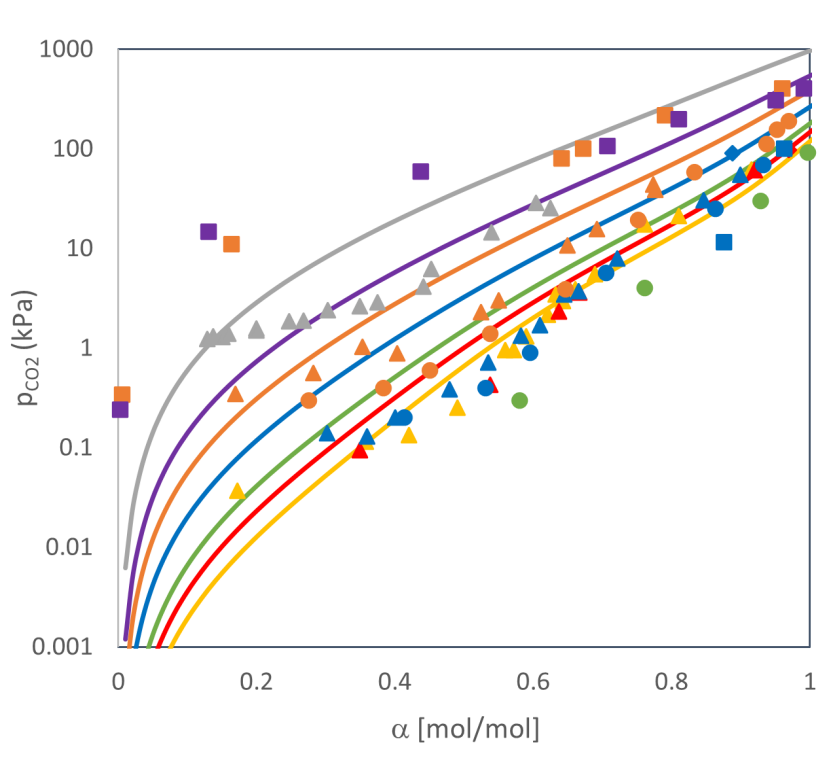

Figure 5.2: Partial pressure of CO_2 as a function of CO_2 loading in 10 wt% SG at temperature between 20 and 78°C. The marker points correspond to the literature values: Song ●, Mondal ■, Harris ◆, Portugal ▲.

The average deviation of the literature and the simulation values for each literature is shown in Table 5.1. For the SG solvent Mondal et al. [49] and Harris et al. [50] have the lowest deviation while for the CESAR-1 solvent it is Hartono et al. [51]. Song et al. [52] and Portugal et al. [53] have deviations of approx. 450% and 200%. These values are so large that the validity of the results from the simulation or experiments are questionable.

Table 5.1: Average deviation (AD) for the VLE literature values of the SG-CO_2 and AMP/PZ-CO_2 systems.

Literature	**Solvent**	**AD [%]**
Song et al.	SG	453.3
Mondal et al.	SG	64.4
Harris et al.	SG	52.0
Portugal et al.	SG	218.9
Hartono et al.	AMP/PZ	23.8
Brúder et al.	AMP/PZ	30.8
Yang et al.	AMP/PZ	123.9
Yang et al. w/o 80°C	AMP/PZ	70.5

To get a better overview of the deviations between the simulation model and literature values the absolute deviation is plotted versus temperature in Figure 5.3. In the

figure the scatter points are coloured according to the loading, where light colours represent low CO_2 loading, lowest at 0.0023 mol CO_2/ mol solvent, and dark colours represent high CO_2 loading, highest at 1.431 mol CO_2/ mol solvent. From the graph it can be observed that the lower loadings have the highest deviation with the top at over 1000% while the higher loadings are below 200%. In the simulation in this thesis the maximum loading of CO_2 is around 0.6, corresponding to the lighter colours, thus suggesting that for the loading used in the simulation there is very high deviation.

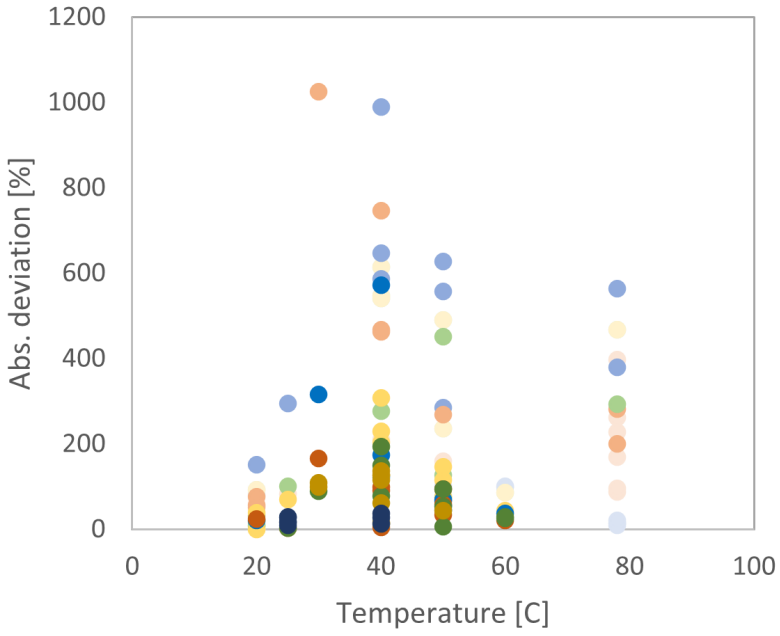

Figure 5.3: Absolute deviation between simulation and literature values for different temperatures. The darker the dataplot the higher loading.

Lastly parity plots for each literature value were plotted for all weight percentages and are illustrated in Figure 5.4. The graph has simulated values plotted as a function of literature values and for illustration purpose the perfect model a x=y line was added as a reference. From the figure it can be seen that Song et al. [52] and Portugal et al. [53] scatter plots are mainly above the xy-line suggesting that the simulation gives too low values, while the values from Mondal et al. [49] shows that the simulation model tends to have too high values. The experiments done by Harris et al. [50] were done for high loadings therefore few data points from this author are shown.

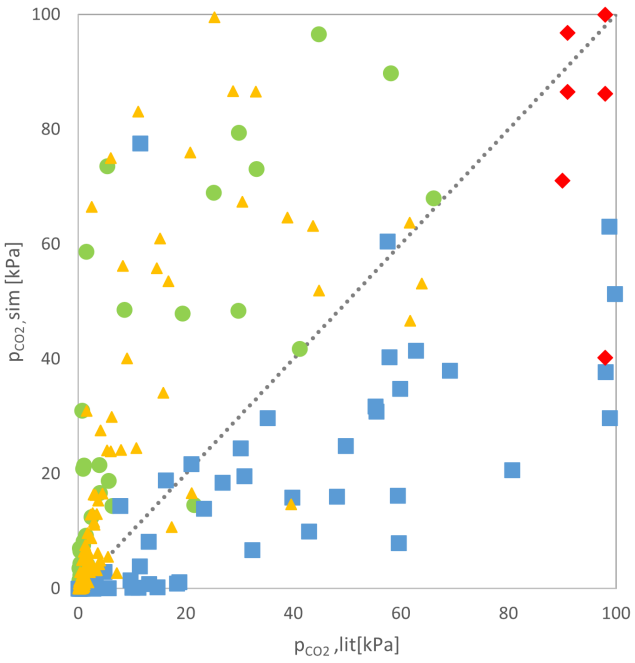

Figure 5.4: Parity plot for calculated CO_2 partial pressure versus experimental CO_2 partial pressure for SG-CO_2 system with 45 wt% SG. The colours correspond to the literature values: Song ● , Mondal ■, Harris ♦ , Portugal ▲

VLE-validation was also done for the AMP/PZ-CO_2 system with 27 and 13 wt% AMP and PZ respectively. Figure 5.5 shows the partial pressure of CO_2 as a function

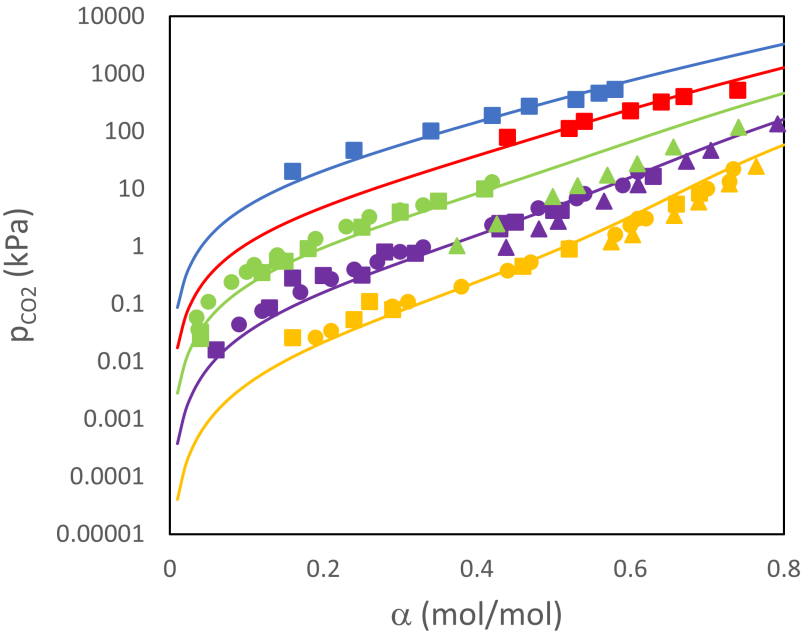

Figure 5.5: Partial pressure of CO_2 as a function of CO_2 loading in 27/13 wt% AMP/PZ at temperature between 40 and 120°C. The marker points correspond to the literature values: Hartono ●, Bruder ■, Yang ▲.

of loading. The partial pressure is shown on a logarithmic scale. In the graph the lines represent the simulation model while the scatter plots represent the literature values. A clear consistency is observed between the simulation and literature values. This is also reflected in the low AD values. The biggest deviation is found between Yang et al. [54] and the model at 80℃ (green line) where the plots are clearly off and do not agree with the other sources. However, as Table 5.1 shows, when disregarding Yang et al. at 80℃ the deviation is reduced from 124% to 71%.

Parity plots for each literature value were plotted and are illustrated in Figure 5.6. The graph have simulated values plotted as a function of literature values and for illustration purpose the perfect model a x=y line was added as a reference. In general there is seen little deviation from the xy-line, but Yang et al. [54] have the highest deviation which correlate to the AD value.

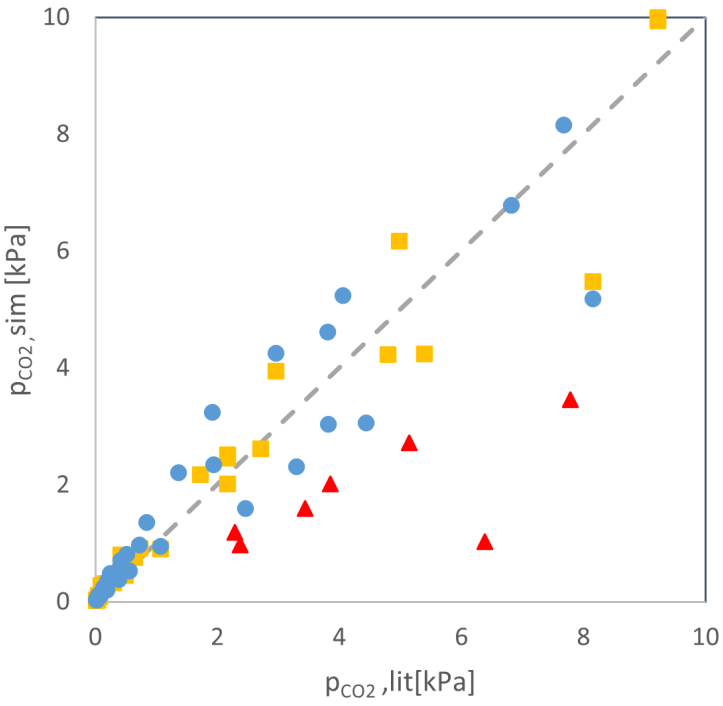

Figure 5.6: Parity plot for calculated CO_2 partial pressure versus experimental CO_2 partial pressure for AMP/PZ-CO_2 system with 27/13 wt% AMP/PZ. The marker points correspond to the literature values: Hartono ●, Bruder ■, Yang ▲

Based on the above results from the SG-CO_2 VLE validation study the simulation results must be read with caution. However since not only the simulation deviates from the literature values, but also the literature values deviate in between themselves, it cannot be decided how to take the deviations into account when viewing the results from the simulation. Protreat did not use any of the experimental data for its model regression, however making a model that coincides with all the experimental

data would be impossible with this high deviation.

The CESAR-1-CO_2 VLE validation study showed in general good fit between the simulation model and experimental data, when excluding Yang at 80℃. Therefore it is assumed that the results found for simulating with the CESAR-1 solvent have high credibiity.

6 Simulation results

In this section the simulation results will be presented. First results from the SG solvent case will be presented, followed by the results from the CESAR-1 solvent simulations.

6.1 Sodium Glycinate solvent base case

A base case of biogas upgrading and cleaning using absorption based technology with AAS SG at 45 wt% was performed. The simulation flow diagram is illustrated in Section 3.1. The base case was simulated with a biogas composition of 3 mol% H_2S, 40 mol% CO_2 and 57 mol% CH_4. The goal of the first part of the simulation study was to reach the upgrading target of 1 mol% CO_2 without specifying the H_2S in the sweet gas. The specific reboiler duty was plotted as a function of L/G-ratio

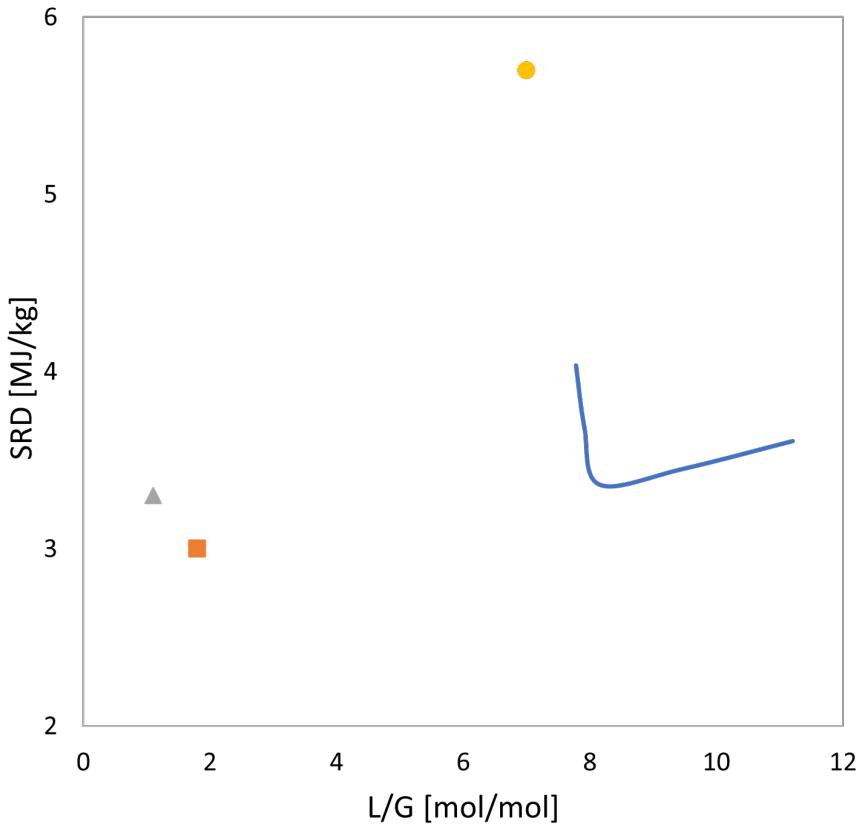

Figure 6.1: Specific reboiler duty as a function of L/G-ratio for the base case with 45 wt% SG solvent. Also the optimal operating point for Weiland et al. [55] as ■, Ogawa [56] as ▲ and Rabensteiner et al. [47] as ●.

and is shown in Figure 6.1. In the figure the optimal operating points from simulation studies by Weiland et al. [55] and Ogawa [56] with 45 wt% SG, and from a pilot plant by Rabensteiner et al. [47] with 40 wt% SG are plotted.

The SRD curve has a typical form where the reboiler duty has two corresponding L/G flow rates in addition to one minimum point. The liquid/gas flow rates above the minimum point have more solvent than needed and thus the reboiler is using energy to increase the temperature of the solvent. For liquid/gas flowrates below the minimum point there is too little solvent in the system, therefore the solvent needs to be regenerated deeper to meet the same specifications. The minimum point corresponds to the balance between too high and too low solvent flow rates and is the optimal operation condition. The minimum specific reboiler duty was found to be 3.36 MJ/kg acid gas at L/G-ratio 8.15 mol/mol.

Weiland et al. reported a regeneration energy of 3 MJ/kg CO_2 at L/G-ratio 1.8 mol/mol and similar results were found by Ogawa with a regeneration energy of 3.3 MJ/kg CO_2 at 1.1 mol/mol. The optimum regeneration energies are similar for the simulations however the L/G-ratio found in this study was much higher than the literature studies. This may be because of higher CO_2 content in the biogas, 40 mol%, compared to Weiland et al. and Ogawa who simulated with flu gas of 13 mol% and 4.72 mol% CO_2 respectively. Furthermore, an increase in circulating flow would requires more pump power and increase the load on the reboiler. The data from Rabensteiner et al. [47] comes from a power plant test facility and shows much higher specific reboiler duty than the simulated values. Also in this case the inlet CO_2 value is lower than the biogas, at 11 vol%. Though the pilot plant used 40 wt% SG solvent it is not expected that a 5 wt% increase would lower the SRD to the simulated values in this study. The VLE validation showed that the model in the simulation program did not correlate to experimental values. The differences in the SRD values are a further indication that this is correct. It should be noted that none of the other studies had a combination of CO_2 and H_2S in the inlet gas, however since the amount of H_2S in the sweet gas was not controlled in this part of the simulation study, this is disregarded.

The H_2S concentration in the sweet gas was not specified in the simulation to observe how it changes for different L/G-ratios. This is shown in Figure 6.2 where the H_2S concentration is plotted as a function of L/G-ratio. At low L/G-ratio the H_2S concentration is high, reaching a peak of 14 000 ppm at around 8 mol/mol while the lowest value is approximately 2 500 ppm at 11.2 mol/mol. High liquid circulation increases the amount of H_2S absorbed, but also increases the reboiler duty.

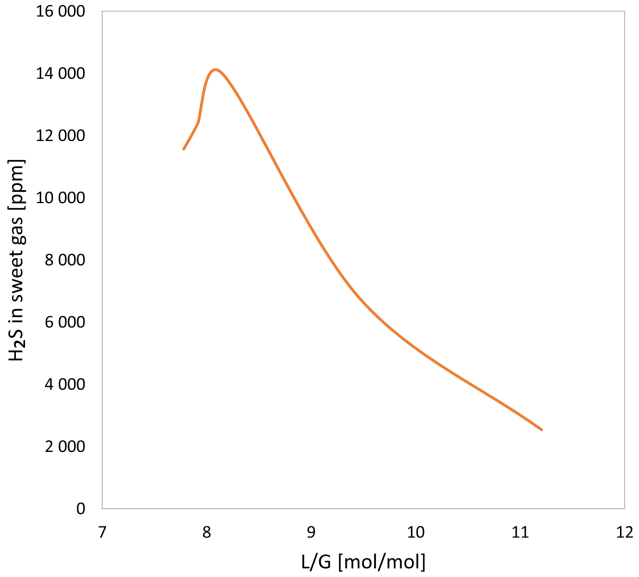

Figure 6.2: H_2S concentration in the sweet gas as a function of L/G-ratio for the base case with 45 wt% SG solvent

The rich and lean loadings of CO_2 and H_2S for L/G-ratio are illustrated in Figure 6.3 and 6.4. The rich CO_2 loading decreases for increasing L/G-ratios, while the lean loading increases. A decreasing rich loading suggests that more circulation liquid does not increase the amount of CO_2 absorbed. Correspondingly an increase in lean loading suggests that there is not enough residence time in the stripper to remove

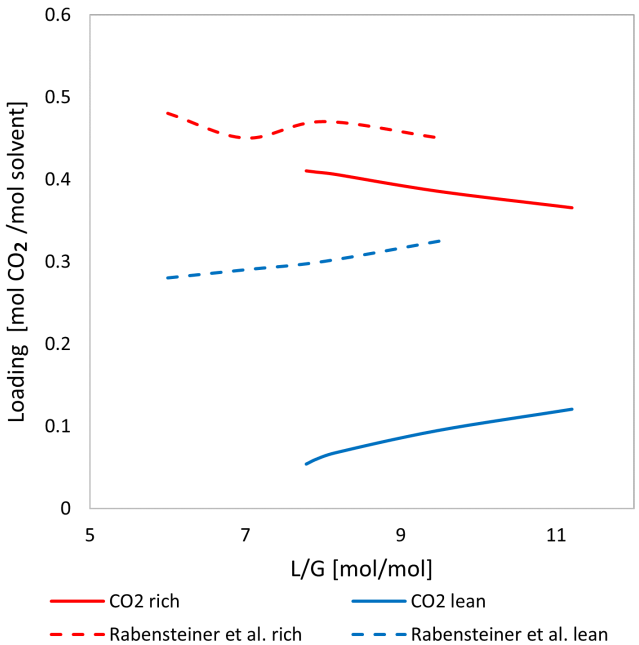

Figure 6.3: CO_2 loading as a function of L/G-ratio for the base case with 45 wt% SG solvent

the CO_2 for higher circulating liquid. The rich and lean loadings for 40 wt% SG found by Rabensteiner et al. [47] are also plotted in Figure 6.3. Both the rich and lean loadings are higher than the simulated values. Especially the lean loading is far greater than the lean loading from simulation. Based on this the simulation model has better CO_2 capture compared to Rabensteiner et al. [47].

Both the rich and lean loading of H_2S increases for increasing L/G-ratio. This means an increasing circulating solvent increases the absorbed H_2S. This can be correlated to the amount of H_2S found in the sweet gas, where a higher L/G-ratio gives lower concentration. The increasing lean loading suggests, such as for the CO_2 lean loading, that the stripper is not removing enough H_2S for higher circulating liquid.

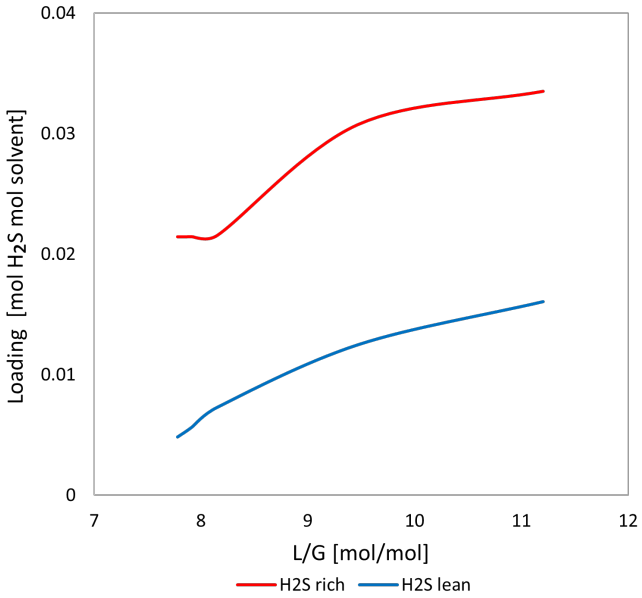

Figure 6.4: H_2S loading as a function of L/G-ratio for the base case with 45 wt% SG solvent

The cyclic capacity of CO_2 and H_2S for the base case is shown in Figure 6.5 where the CC of CO_2 is represented on the left axis and CC of H_2S on the right. The graph shows the CO_2 CC decreases for increasing L/G-ratio, corresponding to lower performance at higher L/G-ratio. The CC of H_2S has a local minimum point at 0.014 mol H_2S/ mol solvent and a maximum point at approximately 0.018 mol H_2S/ mol solvent. The L/G-ratio to the local minimum point corresponds to the highest H_2S concentration in the sweet gas, thus lowest absorption capacity of H_2S. For L/G-ratios higher than 10 mol/mol the CC of H_2S decreases, signifying that the lean loading is increasing faster than the rich loading.

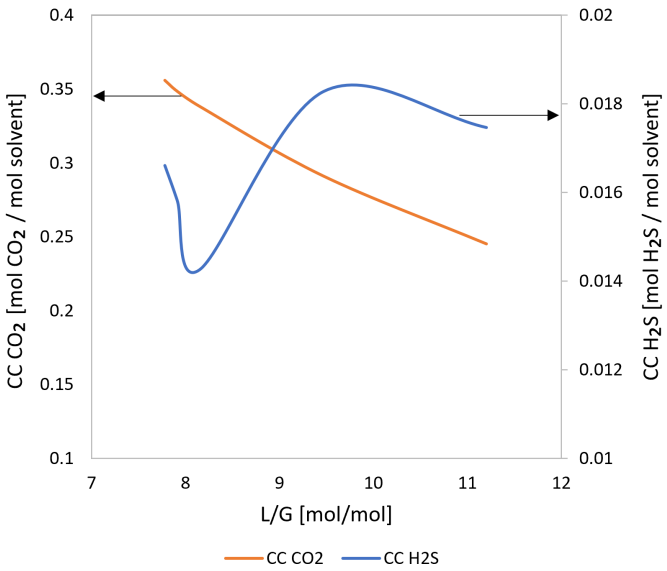

Figure 6.5: Cyclic capacity of CO_2 and H_2S for base case with 45 wt% SG solvent

6.1.1 Variation of absorber height

The effect of changing the absorber column height was investigated by simulating with column heights of 20, 15, 10 and 6 metres. The simulations were done with the specification of 1 mol% CO_2 in the sweet gas. The specific reboiler duty is plotted as a function of column height in Figure 6.6. The different column heights had a similar SRD at approximately 3.5 MJ/kg acid gas, and there is observed a small increase for lower columns. Additionally, the SRD found by Rabensteiner et al. [47] for columns between 12 and 6 metres is plotted for 40 wt% SG and 30 wt% MEA as a comparison. For a 10 metre column it was found that the 40 wt% SG and MEA were respectively 87% and 16% higher than the the 45 wt% SG. It was expected that the regeneration energy would have a greater dependency to column height, as the 40 wt% SG cases from Rabensteiner et al. reported. However the SRD is more similar to the 30 wt% MEA and shows that the regeneration has little dependency to column height.

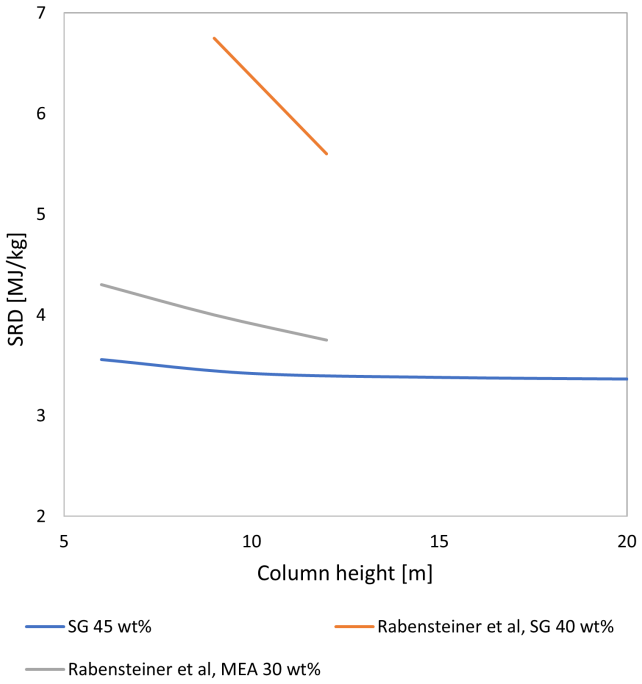

Figure 6.6: Specific reboiler duty as a function of column heights simulated values and literature values from Rabensteiner et al. at 40 wt% SG

The H_2S concentration was found to decrease for decreasing column heights with the lowest value in the 6 metre column at approximately 5 500 ppm, a reduction of approximately 8 500 ppm compared to the 20 metre column. After further investigation of the absorption in the absorber column it was found that for the taller columns desorption occurs in the bottom part of the column. Higher column means that more CO_2 is absorbed and therefore the pH decreases in solution. Figure 1.7 in the introduction shows how the dissociation of H_2S is dependent on the pH. For pH lower than 9 desorption of H_2S occurs. The pH in the columns were investigated and it was found that in all column heights the pH was lower than 9, and it decreased for taller columns. It was also investigated if there would be a difference in changing the stripper height together with the absorber height, but there was found little significance to the stripper energy demand.

The solver function was used to define the sweet gas H_2S concentration to reach the NG requirement. It was found that the simulation could only reduce H_2S to 15 ppm in the sweet gas. Lower values of H_2S did not converge in the simulation program. Figure 6.7 shows the SRD as a function of column height with a requirement of 15 ppm H_2S in the sweet gas. The 6 metre column had the lowest reboiler at 122 MJ/kg acid gas, a reduction of 5 MJ/kg acid gas compared to the 20 metre column. However, the SRD needed to achieve the NG grid requirements, regardless of the

column height, is excessively large and not feasible in the real world.

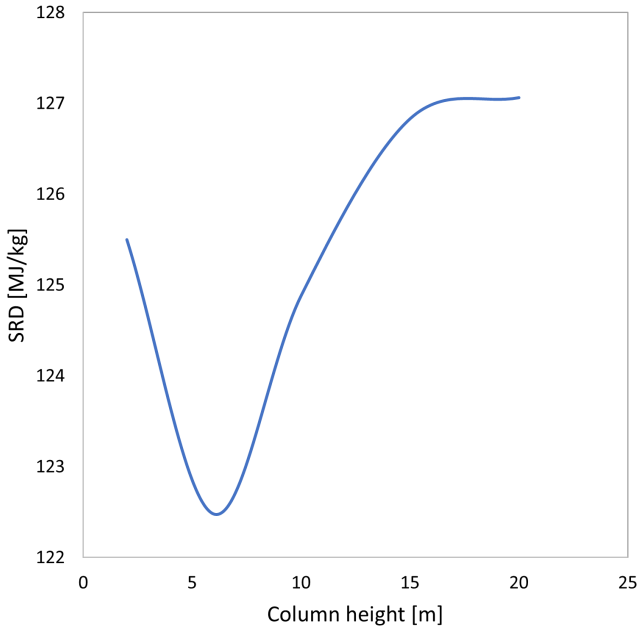

Figure 6.7: Reboiler duty as a function of column heights with solver on H_2S sweet gas at 15 ppm

6.1.2 Variation of inlet stream composition

Reduction of the H_2S in the inlet biogas was tested to see how it affected the system. In the base case a concentration of 3 mol% H_2S was used to simulate biogas with high concentration of H_2S, as the case is for biogas production from vinasse. However, normal H_2S concentrations in biogas are between 80 and 4 000 ppm. Therefore, though the previous simulations have shown SG unfeasible for 3 mol% H_2S concentration in biogas, it was investigated if it can be used for lower concentrations. Simulations were done with an inlet composition of 2, 1, 0.1 and 0.01 mol% H_2S and constant 40 mol% CO_2.

The SRD was found for two cases: specifying 1 mol% CO_2 (upgrading) and specifying 3.578 ppm H_2S (upgrading and conditioning), and is presented in Table 6.1 for the different inlet values. The SRD with the CO_2 specification showed little dependency to the inlet H_2S concentration. This was expected as the amount of CO_2 in the biogas was the same.

When the solver function specified the H_2S in the sweet gas, the cases with 1, 0.1 and 0.01 mol% H_2S were able to reach the NG requirement. Moreover the difference in SRD between only upgrading, and upgrading and conditioning are relatively small for 0.1 and 0.01 mol% H_2S inlets. On the other hand, there is a drastic increase

Table 6.1: Specific reboiler duty with CO_2 requirement and CO_2 and H_2S requirement for different H_2S concentrations in the biogas

Inlet value H_2S [mol%]	**SRD [MJ/kg acid gas] with solver for CO_2 1mol%**	**SRD [MJ/kg acid gas] with solver for H_2S 3.578 ppm**
3	3.36	122 (at 15 ppm)
2	3.37	-
1	3.38	229
0.1	3.39	4.29
0.01	3.40	3.51

from 0.1 to 1 mol% inlet value. The SRD of 1 mol% inlet is 229 MJ/kg acid gas and is approximately twice as large as the SRD found for the base case (3mol%) with 15 ppm H_2S specification. Based on these findings it can be recommended to use SG for upgrading and conditioning of biogas with H_2S content equal or lower than 0.1 mol%. Higher concentrations of H_2S will lead to extremely high regeneration energy.

Nevertheless, as the SRD for 0.1 and 0.01 are similar when removing CO_2 or co-removing CO_2 and H_2S. There is a possibility to use this technology with a desulfursation step before hand to remove the bulk H_2S. therafter AAS absorption can be used for removal of CO2 and H_2S for low content H_2S to make bio-methane. Membranes are known to be good at bulk removal, but also oxygeneration in the digester wil remove alot of H_2S and is very economical.

6.1.3 Study of inter-coolers

The optimal operating point from the base case showed a temperature profile reaching 93℃ in the absorber column. High temperature in the absorber column decreases the rich loading, increases the liquid flowrate required to capture a given amount of acid gas, and consequently increases the regeneration energy needed [25, 57] . It was therefore decided to investigated the usage of ICs to reduce the temperature and subsequently increase amount of acid gas absorbed. As the temperature peak was at the top of the column the placement of the inter-coolers were simulated between 1 to 4 metres from the top.

It was found that the maximum temperature in the absorber column was lower the higher the inter cooler was placed, as shown in Figure 6.8. When the inter cooler was placed 1 metre from the top of the column the temperature was reduced with over 30℃ compared to the optimal operating point without any inter cooler.

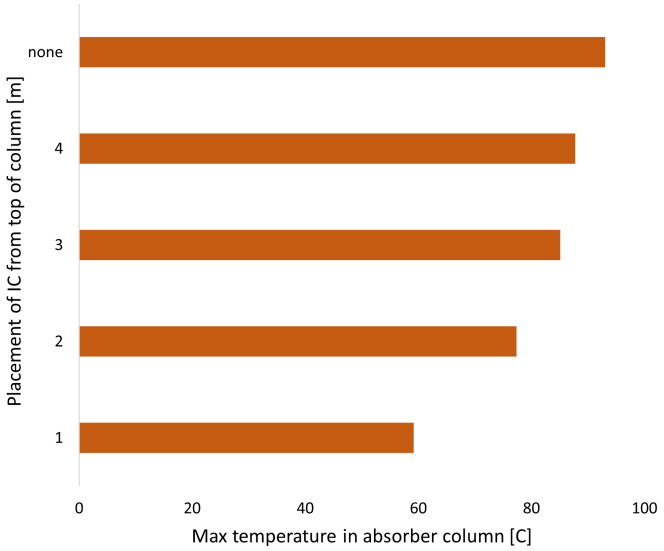

Figure 6.8: Maximum temperature in the absorber column for placement of inter cooler in metres from top.

Introducing an IC gave a small reduction in the specific reboiler duty as shown in Figure 6.9. The optimum SRD with no IC is plotted as a reference. The biggest difference in the SRD is between no IC and IC at 4 metres with 0.34 MJ/kg acid gas, an 11% reduction. A temperature decrease of 30°C resulted in an 11% decrease in SRD, suggesting that further temperature decrease can further reduce the regeneration energy.

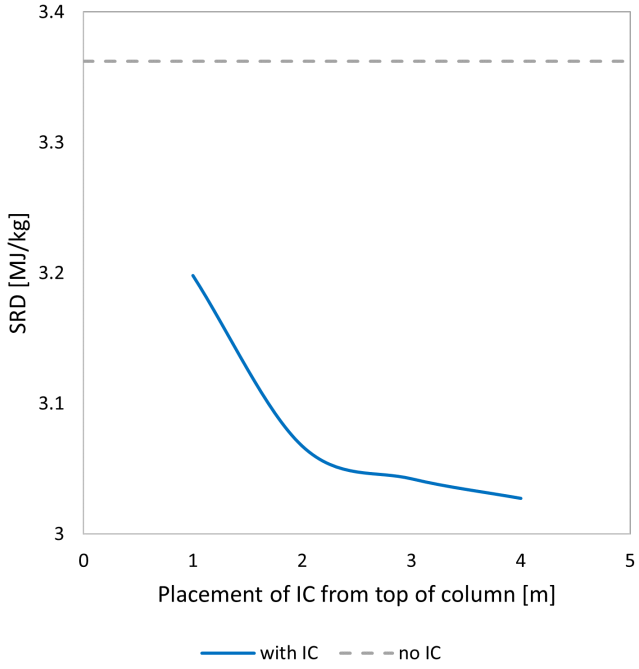

Figure 6.9: Specific reboiler duty as function of IC placement. Line with no IC is shown as a reference.

Figures 6.10 and 6.11 show the lean and rich loading of CO_2 and H_2S as a function of IC placement. The loadings without IC are plotted as reference. It was observed that the acid gas loadings increased when using an IC. Moreover, the rich loadings had a higher increase than the lean loadings, resulting in better cyclic capacity when an IC is used.

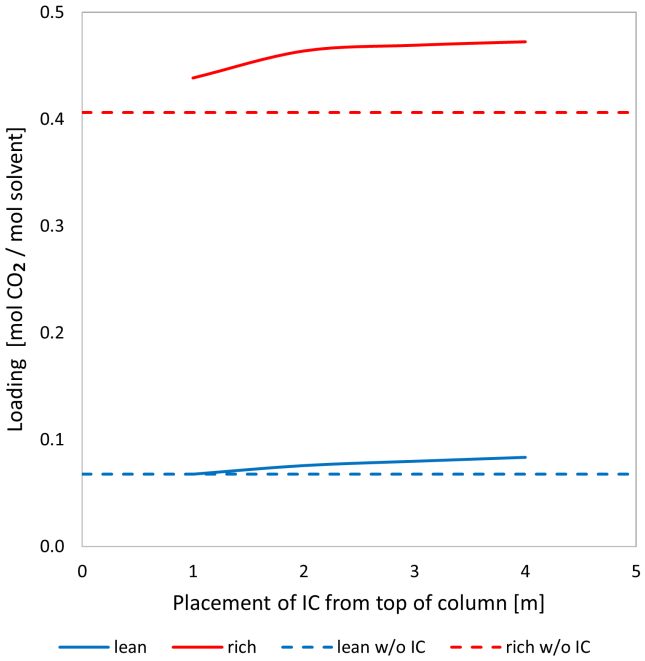

Figure 6.10: CO_2 loading with and without IC for placement of inter cooler in metres from top.

A decrease of 30℃ gave an increase of 0.05 mol CO_2/mol solvent and 0.002 mol H_2S/mol solvent for the rich CO_2 and H_2S loading respectively. The increase in rich loading in addition to lower SRD suggests that integrating IC into the process can be beneficial. Simulations with more IC to reduce the temperature further could show even lower SRDs and higher rich loadings, and were planned to be conducted, however, these simulations were not carried out as the laboratory results showed precipitation issues with 45 wt% SG at low temperatures, see more in Section 4.

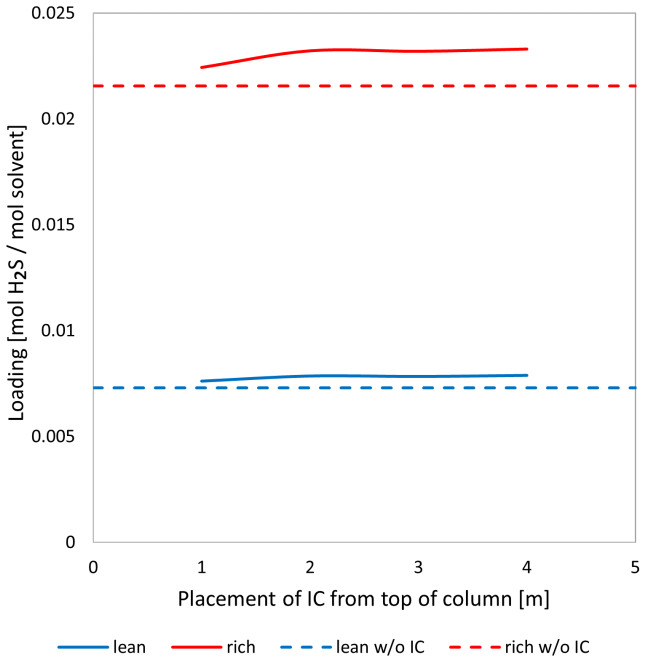

Figure 6.11: H_2S loading with and without IC for placement of inter cooler in metres from top.

6.2 CESAR solvent base case

A base case of biogas upgrading and cleaning using absorption based technology with CESAR-1 (AMP/PZ: 27/13 wt%) solvent was performed. The simulation flow diagram is illustrated in Section 3.1. The base case was simulated with an biogas composition of 3 mol% H_2S, 40 mol% CO_2 and 57 mol% CH_4 in 20 metres absorption and stripper columns. The goal of the simulation study was to reach NG grid requirements of 1 mol% CO_2 and 3.578 ppm H_2S in the sweet gas.

The specific reboiler duty was plotted as a function of L/G-ratio and is shown in Figure 6.12. The figure also includes the SRD from Tobiesen et al. [58] for a 24 and 16.5 metre absorber column with flue gas containing 13.6 mol% CO_2. The optimum operating points form the literature have a SRD of approximately 3 MJ/kg CO_2. Other authors have shown similar results using CESAR-1 solvents [26, 59, 60]. The simulated values in this thesis gave an optimum operating point of 2.6 MJ/kg acid gas at around 5 mol/mol L/G-ratio. The regeneration energy is similar to the literature values, however a much higher L/G-ratio is found in this thesis' simulations. The literature values were from studying flue gases with low CO_2 concentration compared to biogas. Furthermore, Tobiesen et al. [58] does not simulate with H_2S in the flue gas, but this difference is disregarded as the H_2S concentration in the sweet gas was not controlled in the base case.

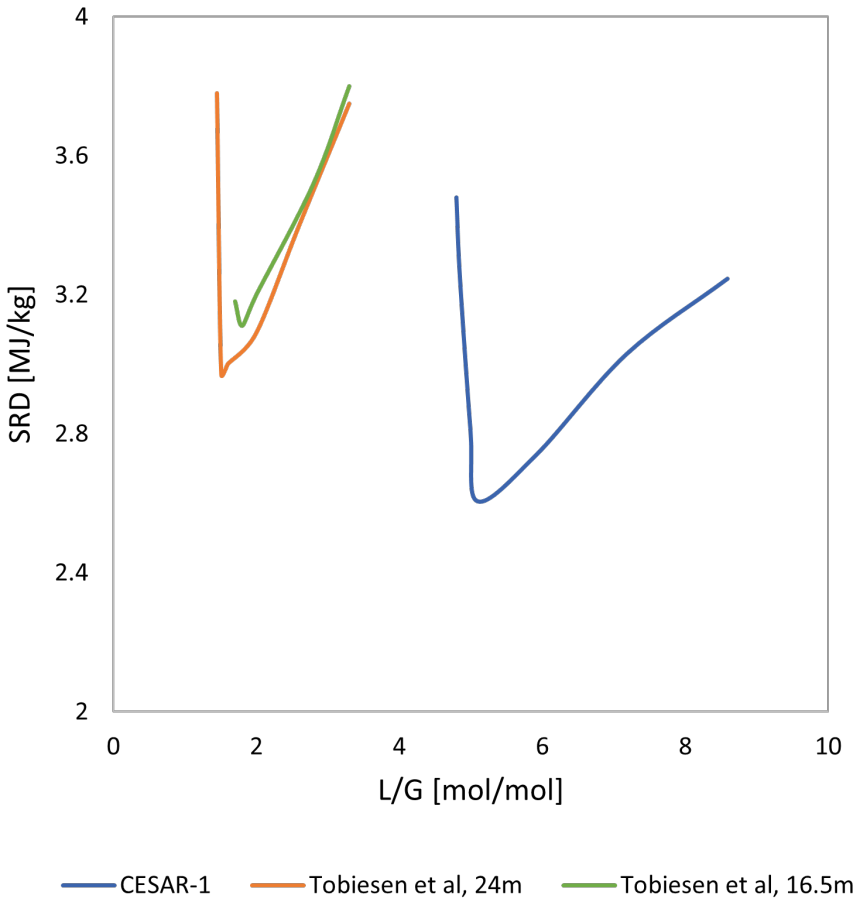

Figure 6.12: Specific reboiler duty [MJ/kg acid gas] as a function of L/G-ratio for the base case of CESAR-1 solvent. SRDs [MJ/kg CO_2] from Tobiesen et al. [58] are plotted as comparison.

The rich and lean loadings of CO_2 and H_2S for L/G-ratio are illustrated in Figures 6.13 and 6.14. It is observed that increasing the L/G-ratio decreases the rich CO_2 loading, and increases the lean CO_2 loading suggesting that increasing the liquid flowrate dose not increase the absorbed CO_2. The optimal operating point gives a rich and lean CO_2 loading of 0.67 and 0.075 mol CO_2/ mol solvent respectively. Tobiesen et al. [58] found that CESAR-1 solvent in 24 and 16.5 metre absorber columns had rich loadings of 0.68 and 0.62 and lean loading of 0.08 and 0.06 for the optimal run. The simulation values of 20 metre column fit well in between the literature values.

In Figure 6.14 the H_2S rich loading has a local maximum point at approximately 0.035 mol H_2S/mol solvent at 6 mol/mol L/G-ratio. Higher and lower L/G-ratios show a decrease in the rich loading. For lower L/G-ratio less H_2S is removed as it is outcompeted by CO_2, while for higher L/G-ratios the increase in liquid flowrate

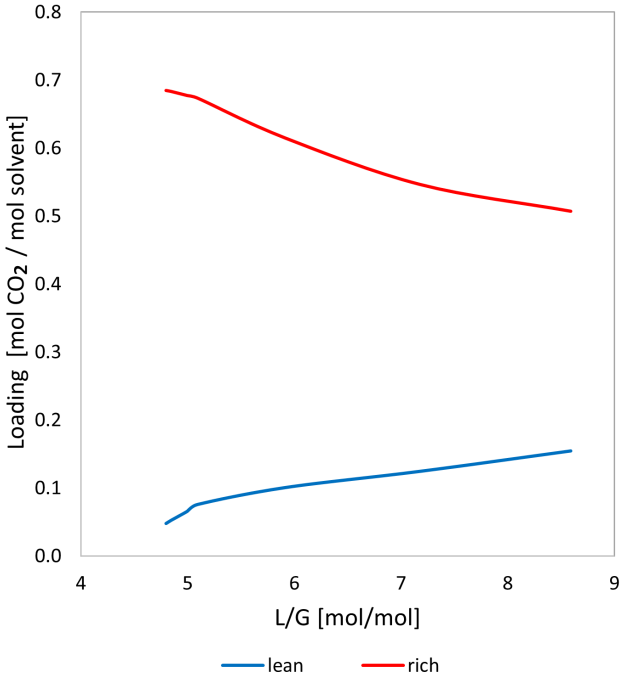

Figure 6.13: CO_2 rich and lean loading as a function of L/G-ratio for the base case of CESAR-1 solvent.

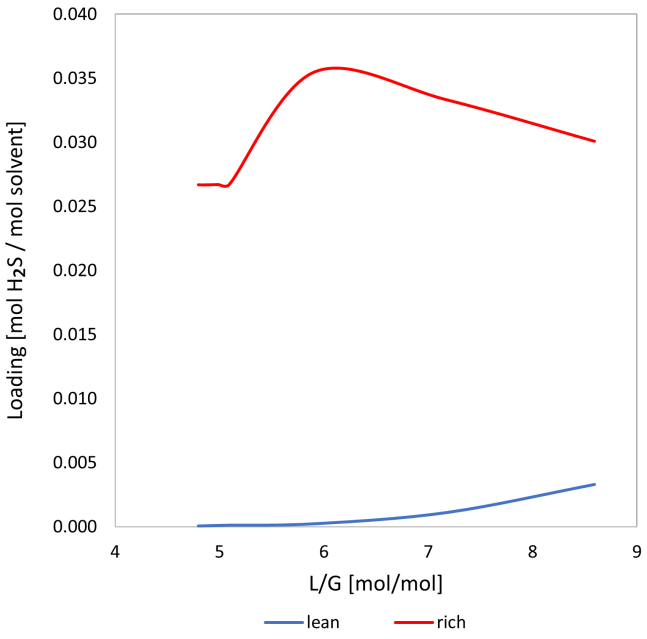

Figure 6.14: H_2S rich and lean loading as a function of L/G-ratio for the base case of CESAR-1 solvent.

is higher than amount of H_2S absorbed. The lean loading has a gentle increase for higher L/G-ratio. The optimal operating point gives a rich and lean H_2S loading of 0.027 and 0.001 mol H_2S/mol solvent respectively.

The results of the change in rich and lean loading can be observed in the cyclic capacity of the acid gases as shown in Figure 6.15, where the CO_2 CC is represented on the left axis and H_2S CC on the right. Furthermore, 4 points are marked on the graph that will be presented in Section 6.2.1. Here it clearly shows that increasing the L/G-ratio decrease the CO_2 absorption, and H2S absorption for L/G-ratio over 6 mol/mol. The local maximum point found for the rich H_2S loading is reflected in the H_2S CC.

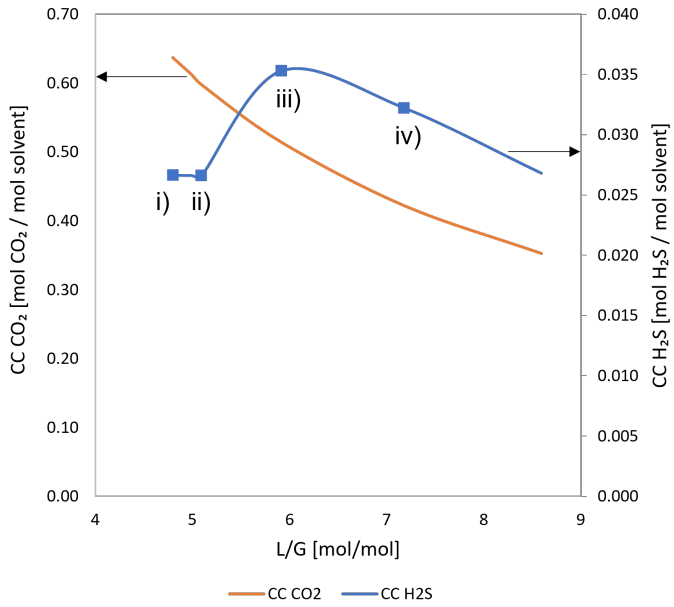

Figure 6.15: Cyclic capacity of CO_2 and H_2S as a function of L/G-ratio for the base case of CESAR-1 solvent.

6.2.1 Investigation of absorber column

The unusual shapes of the rich loading and CC of H_2S found in Figure 6.14 and 6.15 suggest that desorption in the absorption column might be occurring. This was further investigated by looking at the change of partial pressure of the acid gases inside the absorber column. Four points with different L/G-ratios were investigated and are shown in Figure 6.15: i) 4.8 mol/mol the lowest L/G-ratio simulated, ii) 5.1 mol/mol the end of the constant H_2S rich loading at low L/G-ratio, iii) 5.9 mol/mol the top point of H_2S rich loading, and iv) 7.2 mol/mol when the H_2S rich loading is decreasing.

Figure 6.16 illustrates the equilibrium and actual partial pressure of CO_2 as a function of absorber column height for the four cases presented above. The graphs show that for low L/G-ratio, case i) and ii), the actual partial pressure of CO_2 is higher

than the equilibrium partial pressure, and therefore there is a driving force for absorption. The equilibrium and actual partial pressure never meet, and consequently equilibrium is not reached in the column. For higher L/G-ratios, case iii) and iv), equilibrium is meet in the top part of the column. In all cases the actual partial pressure is higher or equal to equilibrium partial pressure, meaning there is no desorption of CO_2 occurring in the column. Furthermore, the highest partial pressure is found at the bottom of the column, signifying that the rich loading is the highest loading in the column. This maximum point of equilibrium partial pressure decreases for higher L/G-ratios which is part of why the CO_2 CC decreases for higher L/G-ratios.

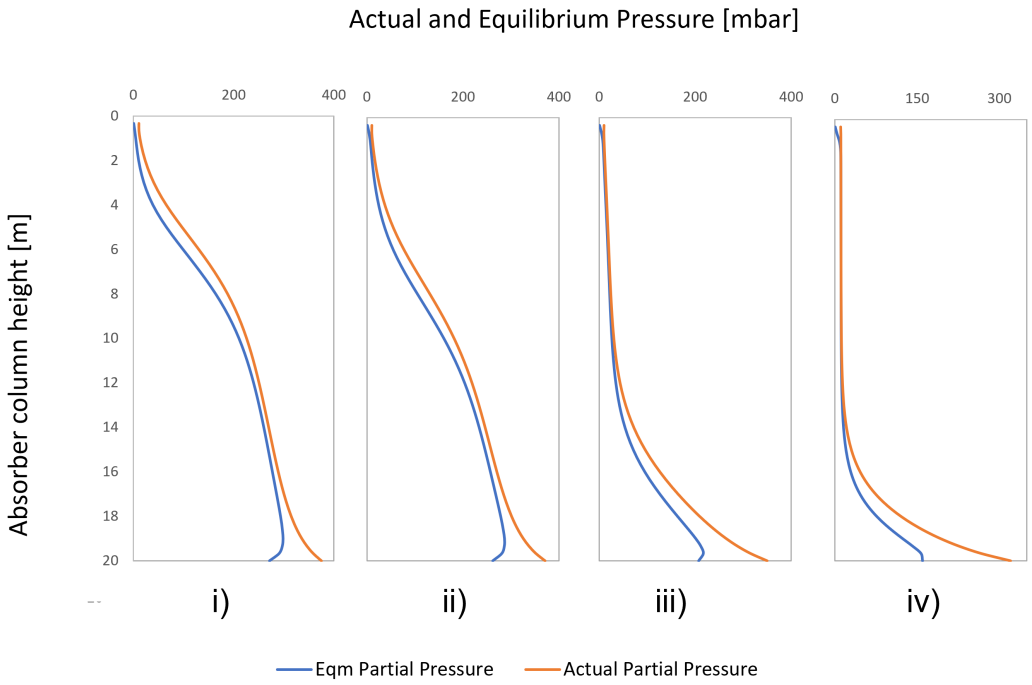

Figure 6.16: Actual and equilibrium partial pressure of CO_2 as a function of absorber column height

The equilibrium and actual partial pressures of H_2S as a function of absorber column height for the four cases mentioned above are shown in Figure 6.17. In the graphs it can be observed that the maximum partial pressure descends in the column for higher L/G-ratios. Furthermore in all cases there is seen absorption, $P^{\text{act}} > P^{\text{eqm}}$, and desorption, $P^{\text{act}} < P^{\text{eqm}}$. However this occurs at different places in the column. Desorption occurs because the actual partial pressure is lower than the equilibrium partial pressure, and does not exceed the maximum point the equilibrium partial pressure has. It is observed that absorption occurs before the maximum point, followed by desorption, and lastly for case i) and ii), equilibrium.

Cases i) and ii) had a similar rich H_2S loading, as illustrated in Figures 6.14 and 6.15, and as the graphs in Figure 6.17 displays, the partial pressures are very similar, there is only a slight descend of the maximum partial pressure in the column. Case iii) had the highest rich loading and the CC of H_2S.

From case iii) to iv) the H_2S rich loading decreases. The partial pressures of case iv) show that in large parts of the column equilibrium is met and there is no driving force for absorption in the upper parts of the column, similar to what was seen for the CO_2 partial pressure. In cases i), ii) and iii) it is observed that at the top of the column there is a driving force, however the actual partial pressure is not high enough, meaning there is not enough H_2S in the biogas, and desorption starts to occur further down the column. In case i) and ii) the desorption occurs quite high in the column, however for case iii), the case with the highest H_2S rich loading, this occurs in the bottom part of the column.

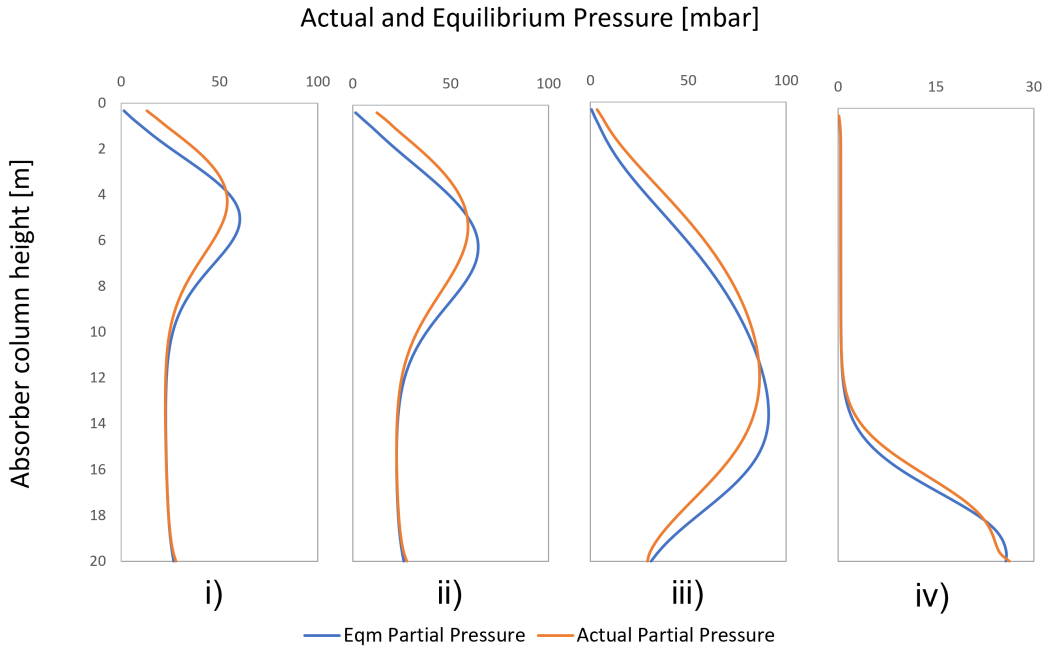

Figure 6.17: Actual and equilibrium partial pressure of H_2S as a function of absorber column height

As mentioned earlier a high pH in the solution is important to absorb H_2S. The pH for the four cases are plotted for the absorber column height in Figure 6.18. The figure shows that the pH varies between 9.5 and 8 down the column, and higher L/G-ratio, that is higher case numbers, have higher pH down the column. In case i) the pH decreases rapidly the first part of the column followed by a stabilising to around 8.2. This corresponds to the section in the absorber where equilibrium is met in the partial pressure of H_2S as illustrated in case i) in Figure 6.17. In case

iv) the first part of the column is mostly constant at a pH around 9, followed by a decrease in the lower part of the column, again similar to the equilibrium in H_2S partial pressure.

A pH around 9 to 10 will fully dissociate H_2S into ions. It must be mentioned when reading Figure 1.7 the scale is in mole fraction. A pH of 8 gives a H_2S mol fraction of 0.1, which corresponds to 100 000 ppm H_2S. Therefore it is critical to keep the pH over 9 to dissociated H_2S into the liquid phase, and a minor decrease of the pH will increase the amount of H_2S in the gas phase significantly.

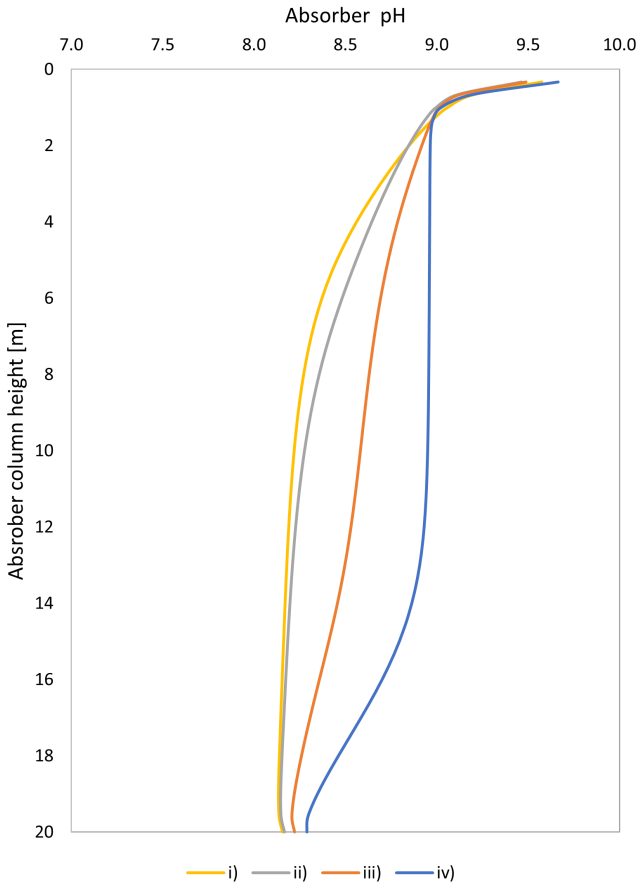

Figure 6.18: pH in the absorber column as a function of absorber column height

Lastly, it cannot be assumed that absorption of the acid gases is independent of each other. This is already shown when analysing the pH, as absorption of CO_2 lowers the pH of the solution substantially. CO_2 is clearly dominant in the biogas and has the advantages of statistically being absorbed more than H_2S just because there are more CO_2 molecules in the gas. In case i) and ii) there is constantly a driving force for CO_2 to be absorbed, thus outcompeting H_2S absorption, for case iii) this is not the fact where equilibrium is meet.

6.2.2 Variation of height

The effect of changing the column heights was investigated by simulating for column heights between 3 and 30 metres. The simulations were done in 2 parts: first with the specifications of 1 mol% CO_2 (upgrading), and secondly, with specification of 3.578 ppm H_2S (upgrading and conditioning). The two cases will be referred to as CO_2 solver and H_2S solver in the following section.

The graph in Figure 6.19 shows the SRD for CO_2 solver and H_2S solver cases as a function of column height. The specific reboiler duty for the CO_2 solver is approximately constant for columns between 10 and 30 metres, and for columns lower than 10 metres the SRD sharply increases as the column reduces to 3 metres, reaching a maximum of 7 MJ/kg acid gas. The increase in reboiler duty is expected because more circulating liquid is needed to absorb the same amount of CO_2 and therefore increasing liquid regeneration. The H_2S solver was only able to meet the NG grid requirements for columns higher than 13 metres. The SRDs were approximately constant at around 4.3 MJ/kg acid gas for all column heights in the H_2S solver case. In both cases for taller columns the SRD is constant. There is a 60% increase from only removing CO_2 to co-removal of CO_2 and H_2S from the biogas for columns higher than 15 metres. The constant SRD for taller columns suggest that after a

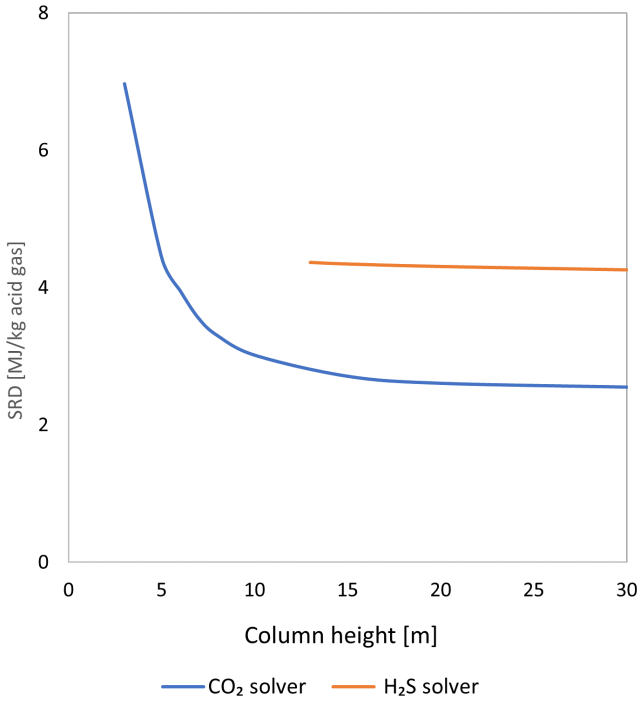

Figure 6.19: Specific reboiler duty as a function of variation in column height

certain height more circulating liquid flow is unnecessary to achieve the sweet gas specifications. Therefore using taller columns, such as 20 or 30 metres, is a waste of process equipment and avoidable increase of CAPEX.

The rich and lean CO_2 loadings from the CO_2 solver and H_2S solver cases are plotted for column heights in Figure 6.20. For the CO_2 solver the rich loading increases for taller columns. The highest loading is found between 10 and 30 metre columns at approximately 0.68 mol CO_2/ mol solvent. The lean loading has a gentle decrease for taller columns. For the lower columns more circulating liquid is needed to have enough residence time, therefore the CO_2 absorption capacity decreases. The rich loading for the H_2S solver case is constant at 0.45 mol CO_2/ mol solvent while the lean loading has a similar decrease as found in the CO_2 solver case. It is observed that the values become constant for taller columns, as remarked upon for the SRDs above. The lower rich loading in the H_2S solver case compared to the CO_2 solver case reflects the increase in solvent required for removing H_2S in addition to CO_2.

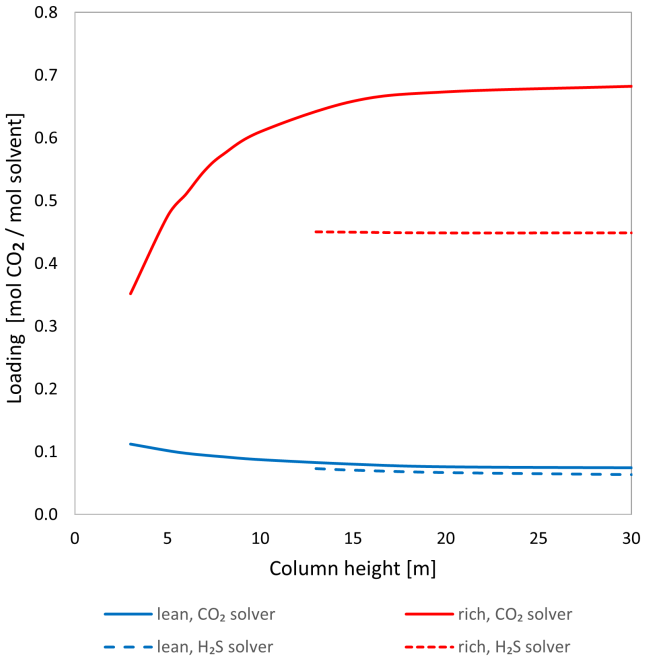

Figure 6.20: CO_2 rich and lean loading as a function of column height.

Similar to the base case the rich H_2S loading for the CO_2 solver case has a local maximum loading as shown in Figure 6.21. The maximum point is located between column heights of 8 and 15 metres. For taller columns the rich loading decreases before becoming constant at 0.027 mol H_2S/mol solvent. For lower columns the rich loading decreases sharply, suggesting that though a lot of H_2S is removed from the biogas, there is a lot of circulating liquid that is not used. The lean loadings for both cases have a similar shape to that of CO_2 lean loading. The rich H_2S loading

from the H_2S solver case is approximately constant at 0.028 mol H_2S/mol solvent. It is observed that the rich loading for the H_2S solver case is higher than the CO_2 solver case. Therefore even though the H_2S solver case has an increase in liquid flow rate, the amount of H_2S removed is much higher than in the CO_2 solver case for columns higher than 13 metres.

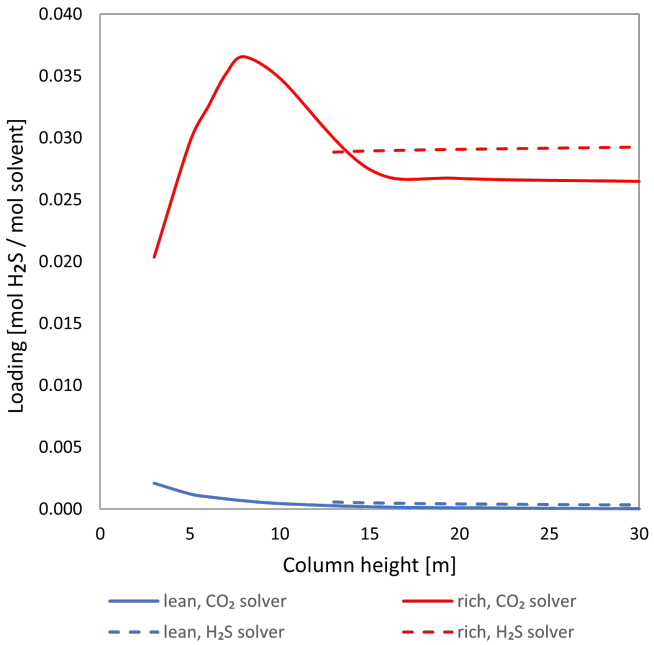

Figure 6.21: H_2S rich and lean loading as a function of column height.

As in the base case, desorption of H_2S in the absorber column was suspected. Therefore, to understand how H_2S is absorbed, the H_2S loading in the absorber column was plotted for the different heights as illustrated in Figure 6.22. In Figure 6.22a the H_2S loading in the liquid phase is plotted as a function of column height. The different colours represent different column heights used in the simulation. As observed all column heights have a maximum H_2S loading around 7 metres, except the 5 and 6 metre column that are not long enough. The 30 metre column has a maximum loading of 0.12 which is over four times as big as the rich loading leaving the absorber column. The graph clearly shows that desorption of H_2S in the column occurs as the loadings decrease down the column. Furthermore, the graph shows that simply reducing the column height to stop the desorption only slightly increases the rich loading.

In Figure 6.22b the difference between increasing or decreasing the stripper height with a constant absorber height of 10 metre is visualised. Increasing the stripper to 30 metres increases the maximum loading in the absorber, but the outlet loading is lower than the 10-10 metre columns. On the other hand, decreasing the stripper height gives a lower max loading, but a slightly higher rich loading. This suggests

that an optimum ratio between absorber and stripper height might be possible to find to increase the amount of acid gas absorbed.

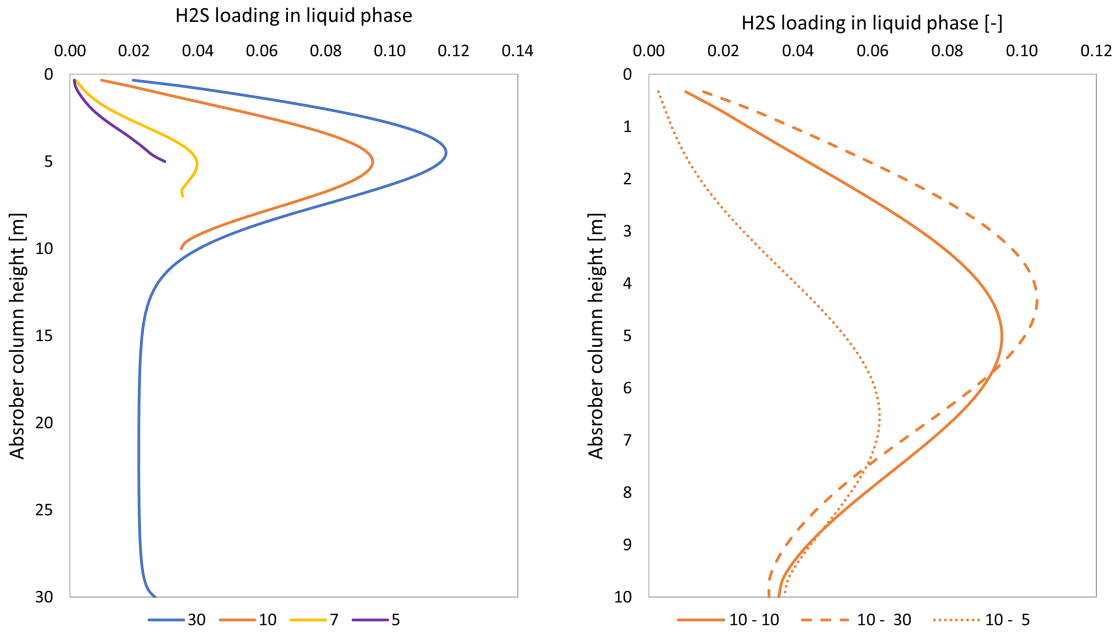

(a) Column heights of 30, 10, 8, 7, 6 and 5 metres

(b) 10 metre absorber column with stripper heights of 5, 10 and 30 metres.

Figure 6.22: H_2S loading in the liquid phase as a function of absorber column height.

In addition to analysing the loading in the column heights the pH in the absorber columns were investigated and is shown in Figure 6.23. The taller columns have higher pH at the top of the column than lower ones. The 30 metre column has a pH of over 10, indicating that no H_2S is in the gas phase and even S^--ions are present. This explains why the taller columns are able to get a maximum loading around 5 meters down the absorber column. The reason for the decrease in loading after this maximum point is that the pH decreases down to approximately 8.2, driving the formation of H_2S again. It is clear that maintaining a high pH is crucial for absorbing H2S regardless of column height and type of solvent.

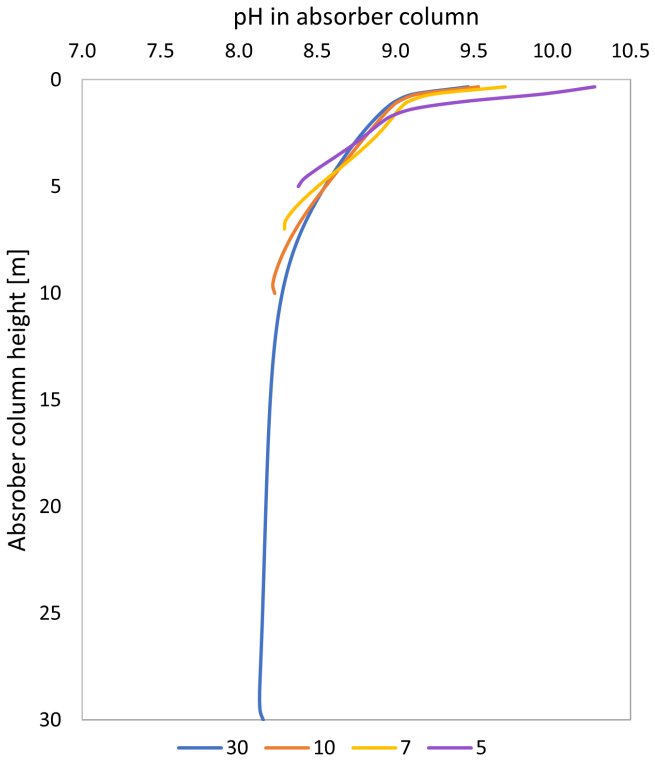

Figure 6.23: pH in the absorber column as a function of absorber column height.

6.2.3 Variation of inlet stream composition

Reduction of the H_2S concentration in the biogas was simulated to see how it affected the system. In the base case a concentration of 3 mol% H_2S was used to simulate biogas with high concentration of H_2S. However, normal H_2S concentrations in biogas varies between 80 and 4 000 ppm. Therefore though the previous simulations have shown CESAR-1 solvent only can reach the NG grid requirement for columns taller than 13 metre, it was investigated if lower columns can be used for lower concentrations.

Simulations were done with 2, 1, 0.1 and 0.01 mol% H_2S and constant 40 mol% CO_2. The specification of 1 mol% CO_2 in the sweet gas was used in the beginning for simulating base cases for each inlet composition. The specific reboiler duty was found to be similar for all cases and the optimal operating points were approximately 2.6 MJ/kg acid gas acid gas at 5 mol/mol L/G-ratio. The similarity was expected as the amount of CO_2 in the biogas was constant and the H_2S concentration changed by 1 to 2%. This is visualised in Figure 6.24 where the specific reboiler duty is plotted as a function of L/G-ratio for all inlet compositions simulated. As the figure illustrates the SRD showed little dependency on the inlet H_2S concentration.

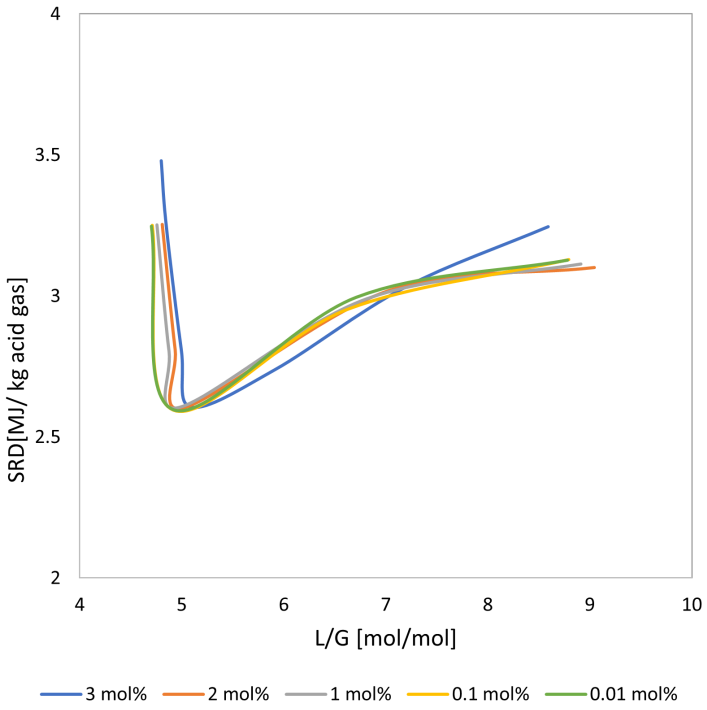

Figure 6.24: The specific reboiler duty as a function of column height

The cyclic capacities were found for each case and are plotted in Figure 6.25 and 6.26 for CO_2 and H_2S accordingly. As the concentration of CO_2 in the inlet is constant and CO_2 was specified in the outlet sweet gas the CC of CO_2 are similar for all cases as shown in Figure 6.25.

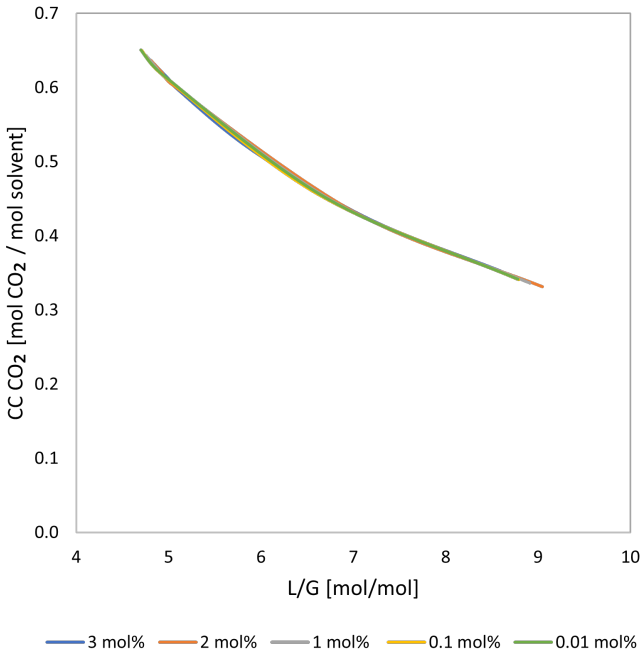

Figure 6.25: Cyclic capacity of CO_2 for different inlet compositions with sweet gas 1mol% CO_2 as a function of L/G-ratio.

The CC of H_2S decreases for lower inlet concentrations of H_2S as there is less H_2S molecules to remove. Additionally, the maximum point found for inlet 3 mol% H_2S flattens out for decreasing inlet values. Therefore for lower inlet values of H_2S there is no difference in capacity for capturing H_2S over different L/G-ratios.

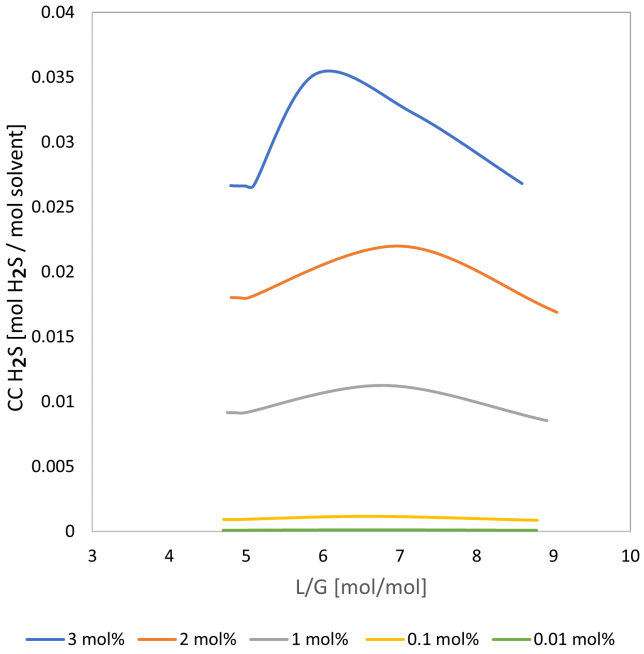

Figure 6.26: Cyclic capacity of H_2S for different inlet compositions with sweet gas 1mol% CO_2 as a function of L/G-ratio.

After the optimum operating points were found, simulations for each inlet composition with lower column heights were preformed. A specification of 3.578 ppm H_2S in the sweet gas was used. Figure 6.27 shows the specific reboiler duty as a function of column height. Each colour corresponds to the inlet value of H_2S and stops at the column height the H_2S requirement no longer can be maintained. The optimum operating points found for the 20 metre columns for each inlet are visualised as one point in the graph.

The figure shows that lower inlet concentrations of H_2S are able to use lower columns to reach the NG requirement. The additional energy needed to remove the H_2S compared to only CO_2 for the 20 metre columns are approximately 1.6 MJ/kg acid gas for the 3, 2 and 1 mol% H_2S inlet cases, and is approximately the same for 0.1 and 0.01 mol% inlet H_2S. Thus for 20 metre columns there is no significant difference between just removing CO_2 and co-removal of CO_2 and H_2S for 0.1 and 0.01 mol% inlet H_2S cases. It is further observed that the SRDs are more or less constant between 20 and 10 metres, suggesting that lower columns can be used without increasing needed energy.

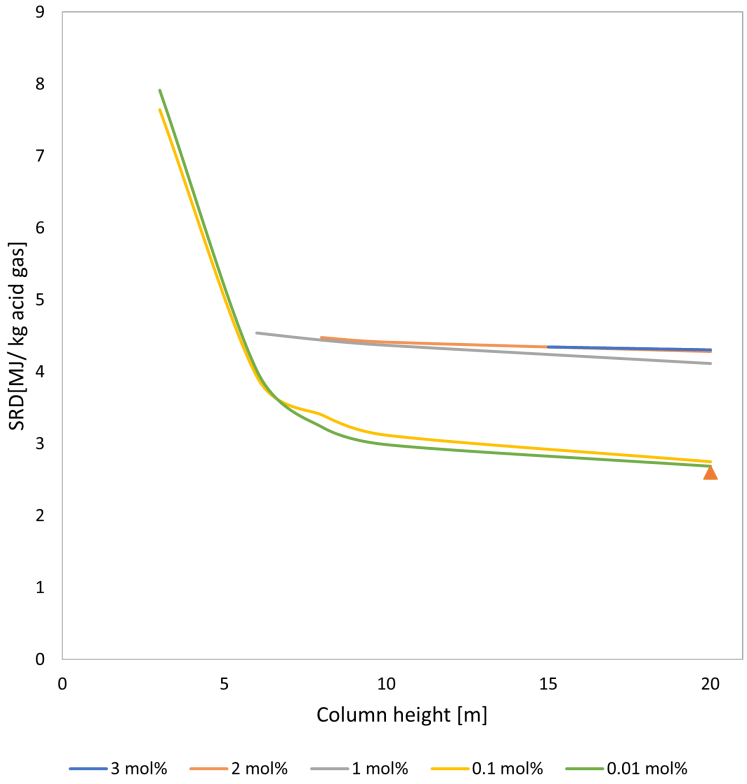

Figure 6.27: The specific reboiler duty as a function of column height for different inlet compositions. ▲ represent the optimum operating point from the base cases.

When decreasing from 10 to 3 metre columns a clear increase in the reboiler duty is observed, making it more energy intensive to remove H_2S from the lower H_2S inlet values compared to the higher inlet values. For the 3 metre columns a SRD of a 8 MJ/kg acid gas was found. Therefore, using columns below 10 metres is not beneficial.

The cyclic capacity of CO_2 and H_2S for the different inlet values when meeting the NG requirement are plotted for column heights in Figure 6.28 and 6.29. The H_2S CC are constant for each inlet value over different column heights as the amount of H_2S is specified in the sweet gas. However since the inlet composition decreases, a decrease in CC is found as well. The highest CO_2 CC values are found for 0.1 and 0.01 mol% H_2S inlet values for the tallest columns. The rich and lean loading of the 20 metre column with 0.01 mol% is 0.68 and 0.08 mol CO_2/ mol solvent respectively. It is also worth mentioning that for the 0.1 and 0.01 mol%, columns lower than 6 and 10 metres receptively are limited by the CO_2 requirement rather than H_2S. They required higher L/G-ratios to reach the 1 mol% CO_2 target over the 3.5 ppm H_2S target which can explain why the cyclic capacity decreases for these column heights.

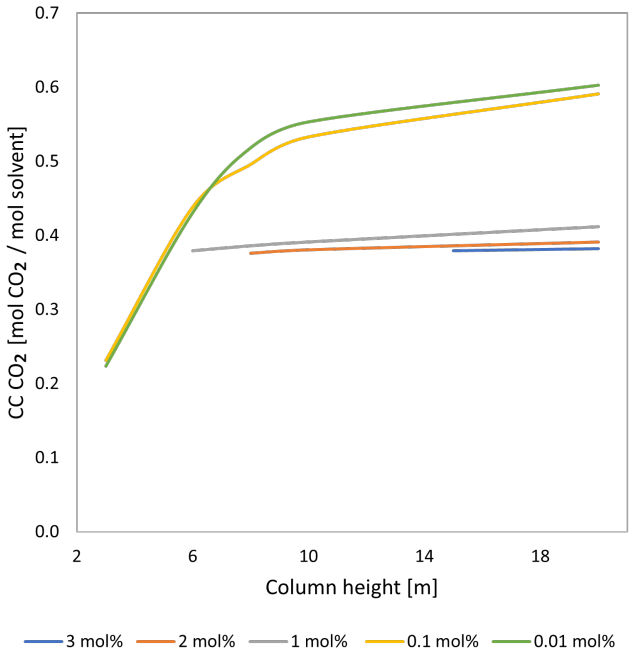

Figure 6.28: Cyclic capacity of CO_2 for different inlet compositions with sweet gas 3.5ppm H_2S as a function of column height

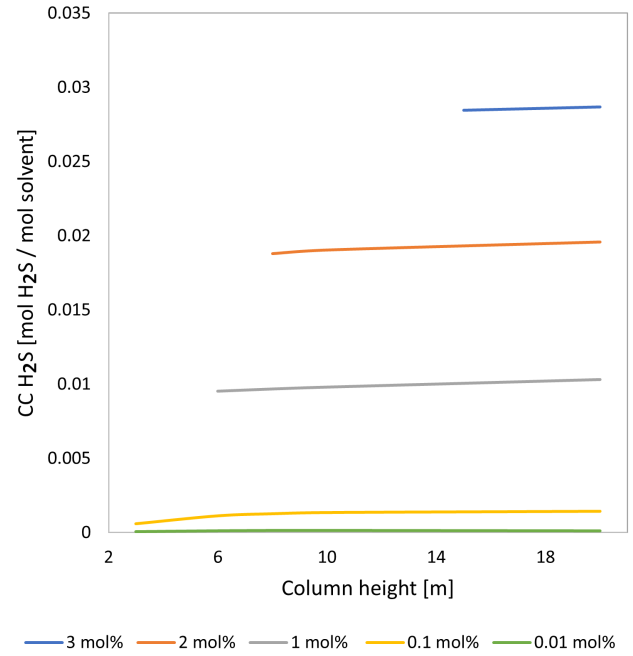

Figure 6.29: Cyclic capacity of H_2S for different inlet compositions with sweet gas 3.5ppm H_2S as a function of column height

7 Economic Analysis

The fixed capital cost (FCC) was found by estimating the cost of equipment and using the Lang factorial method to find the total FCC. For estimating the equipment cost equation 7.1 was used where S is the size parameter for the equipment and a,b and n are cost consonants [61]. Equation 7.2 was used for estimating the equipment cost for the equipment that was outside the ranges of the size parameter in 7.1. Here A is the size parameter for the equipment and K_1 ,K_2 and K_3 are cost consonants [62]. The parameters used for the cost estimation are shown in Appendix B.

$$C_e = a + bS^n \tag{7.1}$$

$$\log_{10}(C_e) = K_1 + K_2 \log_{10}(A) + K_3[\log_{10}(A)]^2 \tag{7.2}$$

To estimate the remaining ISBL along with Offsites (OS), Design and Engineering (D&E) and Contingency (X) the factorial method was used. To calculate the ISBL, equation 7.3 and 7.4 were used for equipment based on carbon-steel (CS) and stainless-steel (SS) respectively. The equation shows how the ISBL was calculated and Equation 7.5 shows how the FCC (C_{FC}) was calculated. The values and explanation for each variable is described in Appendix B.

$$\sum_{i=1}^{i=M} C_{e,i,CS}[(1 + f_p)f_m + (f_{er} + f_{el} + f_i + f_c + f_s + f_l)] \tag{7.3}$$

$$\sum_{i=1}^{i=M} C_{e,i,SS}[(1 + f_p) + (f_{er} + f_{el} + f_i + f_c + f_s + f_l)/f_m] \tag{7.4}$$

$$C_{FC} = C(1 + OS)(1 + D\&E + X) \tag{7.5}$$

Working capital can be estimated from the ISBL. The Operating Costs are divided into Variable Costs (VC) and Fixed Costs (FC). The variables taken into account in the operating cost can be found in Appendix B

A profitability analysis was done to compare the alternatives. The discounted flow method was used to calculate the pay-back time (PBT), discounted net present value (DNPV) and the internal rate of return (IRR). The equation used for the calculation

is shown in Appendix B.

7.1 Results economic analysis

In total 6 cases of a economic analysis were done, consisting of two cases with 15 meter columns with inlet H_2S concentration of 3 and 0.1 mol and four cases with 10 meter columns with inlet H_2S concentration of 2, 1, 0.1 and 0.01 mol as presented in Table 7.1.

Table 7.1: Cases analysed in the profitability study

Case	**Column height [m]**	**H_2S inlet [mol%]**
Case 1	15	3
Case 2	15	0.1
Case 3	10	2
Case 4	10	1
Case 5	10	0.1
Case 6	10	0.01

The equipment cost for all cases are presented in Figure 7.1. In the Figure the Absorber and Stripper contains the cost of both the vessel and the packing inside the column. The category "other" contains the cost of the condenser, heat exchanger, coolers, pumps, compressor and flash. In all cases the reboiler the most expensive single equipment ranging between 20 to 23% of the total equipment cost. The absolute cost of each equipment for each case can be found in Appendix B.

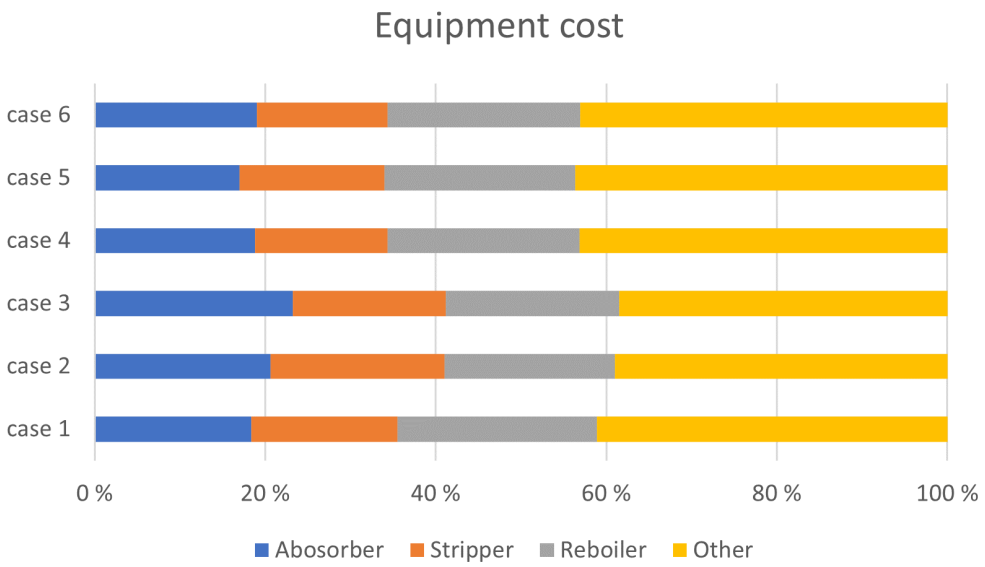

Figure 7.1: Percentages of equipment cost for all the cases analysed in the profitability analysis.

The yearly cash flow for each of the cases evaluated in the profitability analysis is presented Figure 7.2. The Yearly cash flow consists of operational cost, i.e. FC and VC, and the revenues. In all cases is the revenue larger than the operating cost, meaning that each year is profitable.

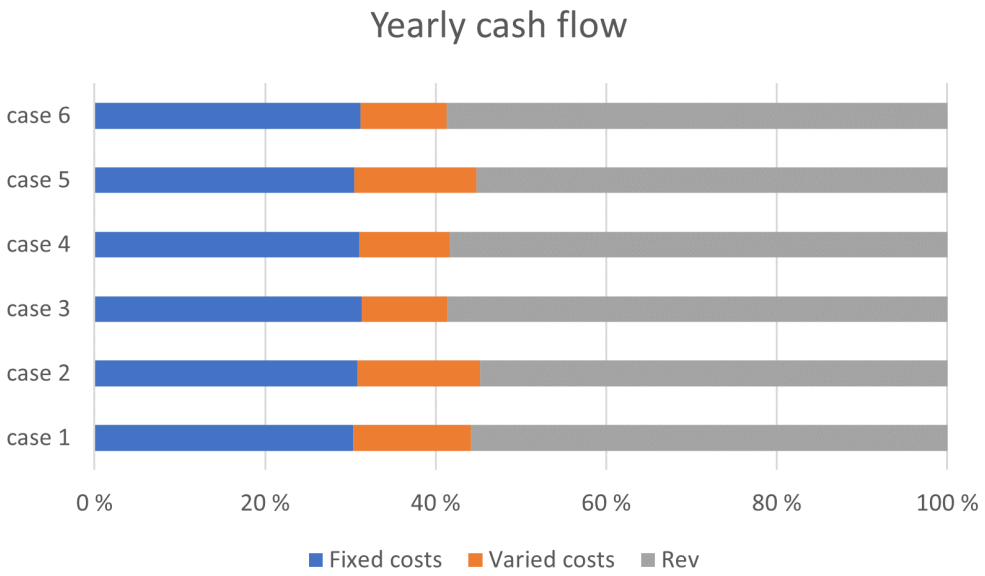

Figure 7.2: Percentages of yearly cash flow as operational cost and revenues.

An overview of the ISBL, DNPV, IRR and PBT for each case is shown in Table 7.2. Cases with the same column height show better profitability for lower concentrations. Furthermore, it seems that the H_2S inlet concentration has a bigger impact on the

ISBL than column height as the ISBL. Comparing case 3 and case 2, it shows that even though case 3 has a taller column case 5 has a larger ISBL. Therefore even though the column height is reduced, since the H_2S inlet is increased the ISBL increases. An explanation for this may be that fact that it was found that 3,2 and 1 mol% had similar reboiler duties, and the same for 0.1 and 0.01 mol%. When comparing case 2 and case 5, that have the same inlet concentration, it is observed that the lower columns give lower ISBL. Therefore it can be assumed that both column height and inlet composition affect the cost of the plant.

Table 7.2: Results from the profitability analysis

Case	ISBL [mill USD]	DNPV [mill USD]	IRR [%]	PBT of [years]		Process parameters	
				NPV	DNPV	L/G [mol/mol]	SRD [MJ/kg]
Case 1	2	-0.4	5.32	8.3	>10	8.2	4.34
Case 2	1.6	2.5	25.59	3.7	4.1	5.4	2.83
Case 3	1.8	0.375	10.62	6.3	8.3	8.2	4.41
Case 4	1.6	0.92	14.58	5.3	6.6	7.9	4.37
Case 5	1.5	2.5	26.5	3.4	3.8	5.8	3.12
Case 6	1.4	2.7	28.22	3.4	3.8	5.5	2.99

It is claimed that processes with higher reboiler duty and higher liquid circulating flow rate require more energy and more/bigger equipment [23] In the table the L/G-ratio and the reboiler duty are shown for each case. The table clearly shows that the cases with highest ISBL (and lowest DNPV) also have highest L/G-ratio and reboiler duty, supporting that L/G-ratio and reboiler duty have a substantial influence on the cost of the plant.

Case 1, using a 15 meter column for 3 mol% H_2S inlet has the worst outcome with the highest ISBL, lowest IRR and a PBT over the estimate lifetime of the plant. Case 6 comes out as the best case with the lowest ISBL, highest IRR and shared PBT with case 4. The DNPV are all positive except for the "worst" case. At best it can be expected to make USD 2.7 million for a plant life of 10 years. The PBT ranges between approximately 4 to over 10 years when based on the DNPV. The net present value (NPV) and the DNPV for the worst and best cases are plotted in Figure 7.3 and 7.4. The PBT is found when the NPV or DNPV becomes positive cash flow.

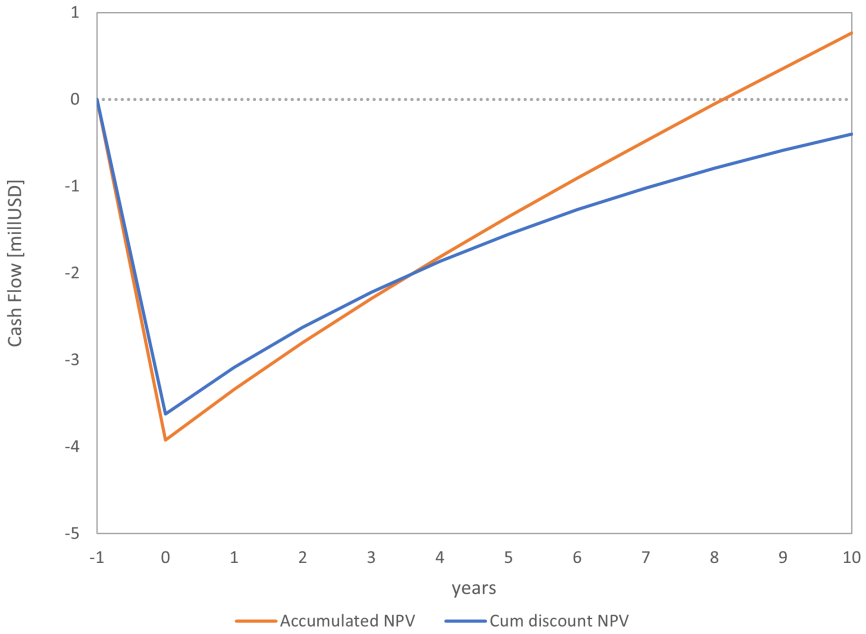

Figure 7.3: NPV and DNPV over years for 15m column with 3 mol H_2S inelt case

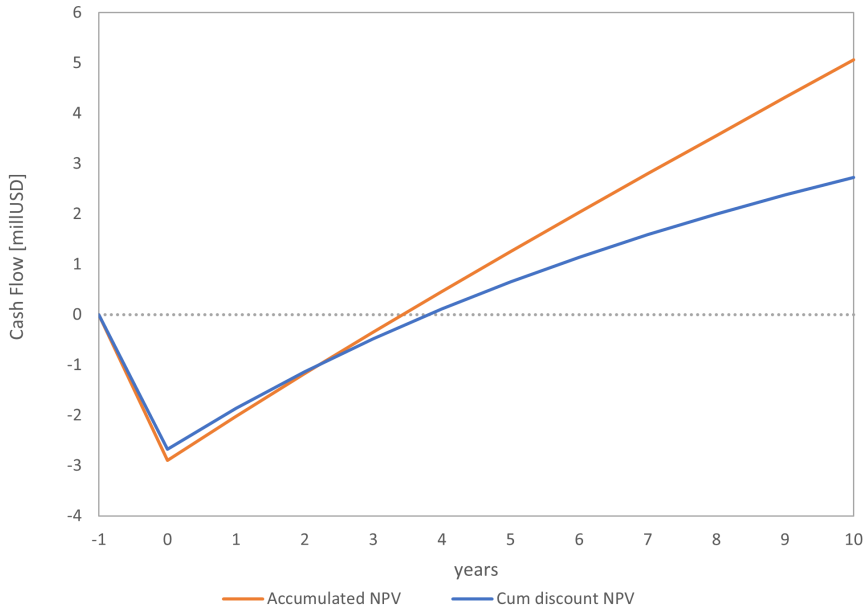

Figure 7.4: NPV and DNPV over years for 15m column with 3 mol H_2S inelt case

It should be noted that certain parts of the treatment line from biogas to the NG grid distribution network were not taken into account. The sweet gas must be further treated: removing water, odrise CH_4 and pressurise it to the NG grid standards. All of these treatments will also cost money. Furthermore, as CO_2 and H_2S are co-absorbed there must be a desulphurisation unit, e.g. CLAUS unit, and CO_2 recovery unit. These units will also cost a lot of money.

8 Conclusion

In this thesis upgrading and conditioning of biogas with high H_2S content to meet the natural gas grid requirement of 1 mol% CO_2 and 5 mg/mL H_2S was studied. Simulations with 45 wt% sodium glycinate and 40 wt% CESAR-1 (AMP/PZ 27/13 wt%) solvents and precipitation experiments of SG were preformed.

Based on published data it was unsure if precipitation of 45 wt% SG would occur as the literature is in disagreement. Precipitation experiments with 45 and 35 wt% SG clearly showed precipitation occurring when CO_2 is absorbed, therefore it cannot be recommended to use these weight percentages for gas-liquid based absorption technology.

The simulation with 45 wt% SG showed that the SRD had a higher L/G-ratio than found in the literature. The SRD value resembled earlier work using Protreat, but was much lower compared to data from a real test facility pilot plant. Furthermore, the VLE-validation showed high deviation to literature data, therefore the results from this simulation was deemed improbable. Therefore even though AAS are better for the environment than amines, the data suggest that SG is not suitable for biogas upgrading and cleaning.

The simulations with 40 wt% CESAR-1 solvent showed that columns taller than 13 metres are able to meet the NG grid requirement with an SRD of approximately 4.3 MJ/kg for biogas with 3 mol% H_2S. Additionally columns down to 3 metres can be used for lower inlet concentrations of H_2S. There were problems with H_2S desorption in all simulation cases, and it was found that maintaining high pH is crucial to absorb H_2S.

A profitability study was done for five simulation cases with varying column height and inlet H_2S composition. The study showed that it is not profitable to co-absorb CO_2 and H_2S from the biogas for a plant with a lifetime of 10 years. However lower columns and inlet H_2S concentrations were profitable, with the "best" case scenario of using a 10 meter column with 0.01 mol% H_2S giving a DNPV of USD 2.7 million, IRR of 29% and PBT of 3 years.

9 Recommendation for further work

More laboratory experiments should be preformed to gain further insight into precipitation of SG and potentially other amino acid salts. Other AAs should be investigated as solvents for biogas upgrading. The results have shown clear differences between flue gas and biogas in SRD, loadings and liquid flowrates. More data should be obtained on biogas upgrading and cleaning to gain further insight.

The observed problems of H_2S desorption in the absorber column should be further investigated. If desorption can be stopped more H_2S can be absorbed and result in a a more optimal process.

Further investigations should be done on separation of the CO_2 and H_2S gas in a desulphurising unit, e.g. CLAUS unit. A profitability analysis of the steps in between the absorption unit and the finished sale gas should be done to get a more realistic picture of the required cost of the process.

References

[1] IEA. World energy outlook 2020, iea, 2020. URL https://www.iea.org/reports/world-energy-outlook-2020.

[2] IEA. Total primary energy supply by fuel, 1971 and 2019, 2019. URL https://www.iea.org/data-and-statistics/charts/total-primary-energy-supply-by-fuel-1971-and-2019.

[3] IEA. World total final consumption by source, 1971-2019, 2019. URL https://www.iea.org/data-and-statistics/charts/world-total-final-consumption-by-source-1971-2019.

[4] IEA. Iea (2020),outlook for biogas and biomethane: Prospects for organic growth, 2020. URL https://www.iea.org/reports/outlook-for-biogas-and-biomethane-prospects-for-organic-growth.

[5] European Commission. Com(2022) 230 final. May 2022.

[6] Margareta Persson. Evaluation of upgrading techniques for biogas. Technical report, Swedish Gas Center, 2003.

[7] Laura Alllegue and Jørgen Hinge. Biogas and bio-syngas upgrading. Technical report, Danish Technological Institute, December 2012.

[8] Arthur Wellinger and Anna Lundberg. Biogas upgrading and utilisation. Technical report, IEA, 2013.

[9] Arthur L. Kohl and Richard B. Nielsen. Chapter 11 - absorption of water vapor by dehydrating solutions. In Arthur L. Kohl and Richard B. Nielsen, editors, *Gas Purification (Fifth Edition)*, pages 946–1021. Gulf Professional Publishing, Houston, fifth edition edition, 1997. ISBN 978-0-88415-220-0. doi: https://doi.org/10.1016/B978-088415220-0/50011-2. URL https://www.sciencedirect.com/science/article/pii/B9780884152200500112.

[10] Laura Alllegue and Jørgen Hinge. Biogas upgrading- Evaluation of methods for H2S removal. Technical report, Danish Technological Institute, December 2014.

[11] Mostafa Parsaee, Mostafa Kiani Deh Kiani, and Keikhosro Karimi. A review of biogas production from sugarcane vinasse. *Biomass and Bioenergy*, 122: 117–125, 2019. doi: https://doi.org/10.1016/j.biombioe.2019.01.034.

[12] United States Department of Labor. Hydrogen sulfide - hazards — occupational safety and health administration, 2022. URL https://www.osha.gov/hydrogen-sulfide/hazards.

[13] J I Huertas, N Giraldo, and S Izquierdo. *7 Removal of H 2 S and CO 2 from Biogas by Amine Absorption.* InTech Europe, 11 2011. ISBN 978-953-307-619-5. URL http://www.intechopen.com/books/mass-transfer-in-chemical-engineering-processes/removal-of-h2s-and-co2-from-biogas-by-amine-absorption.

[14] 2022 Colloide Engineering Systems. What is anaerobic digestion?, 2022. URL https://www.colloide.com/what-is-anaerobic-digestion/.

[15] Mostafa Parsaee, Mostafa Kiani Deh Kiani, and Keikhosro Karimi. A review of biogas production from sugarcane vinasse. *Biomass and Bioenergy*, 122: 117–125, 3 2019. ISSN 0961-9534. doi: 10.1016/J.BIOMBIOE.2019.01.034.

[16] Júlio Cesar de Carvalho, Luciana Porto de Souza Vandenberghe, Eduardo Bittencourt Sydney, Susan Grace Karp, Antonio Irineudo Magalhães, Walter José Martinez-Burgos, Adriane Bianchi Pedroni Medeiros, Vanete Thomaz-Soccol, Sabrina Vieira, Luiz Alberto Junior Letti, Cristine Rodrigues, Adenise Lorenci Woiciechowski, and Carlos Ricardo Soccol. Biomethane production from sugarcane vinasse in a circular economy: Developments and innovations. *Fermentation*, 9, 4 2023. ISSN 23115637. doi: 10.3390/fermentation9040349.

[17] Jorge Vinicius da Silva Neto, Waldyr L.R. Gallo, and Edson Aparecido Abdul Nour. Production and use of biogas from vinasse: Implications for the energy balance and ghg emissions of sugar cane ethanol in the brazilian context. *Environmental Progress and Sustainable Energy*, 39, 1 2020. ISSN 19447450. doi: 10.1002/ep.13226.

[18] Arthur L. Kohl and Richard B. Nielsen. Chapter 1 - introduction. In Arthur L. Kohl and Richard B. Nielsen, editors, *Gas Purification (Fifth Edition)*, pages 1–39. Gulf Professional Publishing, Houston, fifth edition edition, 1997. ISBN 978-0-88415-220-0. doi: https://doi.org/10.1016/B978-088415220-0/50001-X. URL https://www.sciencedirect.com/science/article/pii/B978088415220050001X.

[19] Arthur L. Kohl and Richard B. Nielsen. Chapter 14 - physical solvents for acid gas removal. In Arthur L. Kohl and Richard B. Nielsen, editors, *Gas Purification (Fifth Edition)*, pages 1187–1237. Gulf Professional Publishing, Houston, fifth edition edition, 1997. ISBN 978-0-88415-220-0. doi: https://doi.

org/10.1016/B978-088415220-0/50014-8. URL https://www.sciencedirect.com/science/article/pii/B9780884152200500148.

[20] Arthur L. Kohl and Richard B. Nielsen. Chapter 15 - membrane permeation processes. In Arthur L. Kohl and Richard B. Nielsen, editors, *Gas Purification (Fifth Edition)*, pages 1238–1295. Gulf Professional Publishing, Houston, fifth edition edition, 1997. ISBN 978-0-88415-220-0. doi: https://doi.org/10.1016/B978-088415220-0/50015-X. URL https://www.sciencedirect.com/science/article/pii/B978088415220050015X.

[21] Arthur L. Kohl and Richard B. Nielsen. Chapter 12 - gas dehydration and purification by adsorption. In Arthur L. Kohl and Richard B. Nielsen, editors, *Gas Purification (Fifth Edition)*, pages 1022–1135. Gulf Professional Publishing, Houston, fifth edition edition, 1997. ISBN 978-0-88415-220-0. doi: https://doi.org/10.1016/B978-088415220-0/50012-4. URL https://www.sciencedirect.com/science/article/pii/B9780884152200500124.

[22] G. Puxty and M. Maeder. 2 - the fundamentals of post-combustion capture. In Paul H.M. Feron, editor, *Absorption-Based Post-combustion Capture of Carbon Dioxide*. Woodhead Publishing, 2016. doi: https://doi.org/10.1016/B978-0-08-100514-9.00002-0.

[23] Sajjad Sharif Dashti, Ahmad Shariati, and Mohammad Reza Khosravi Nikou. Sensitivity analysis for selection of an optimum amine gas sweetening process with minimum cost requirement. *Asia-Pacific Journal of Chemical Engineering*, 10(5):709–715, 2015. doi: https://doi.org/10.1002/apj.1907. URL https://onlinelibrary.wiley.com/doi/abs/10.1002/apj.1907.

[24] Ida M. Bernhardsen and Hanna K. Knuutila. A review of potential amine solvents for co2 absorption process: Absorption capacity, cyclic capacity and pka. *International Journal of Greenhouse Gas Control*, 61:27–48, 2017. doi: https://doi.org/10.1016/j.ijggc.2017.03.021.

[25] Arthur L. Kohl and Richard B. Nielsen. Chapter 2 - alkanolamines for hydrogen sulfide and carbon dioxide removal. In Arthur L. Kohl and Richard B. Nielsen, editors, *Gas Purification (Fifth Edition)*, pages 40–186. Gulf Professional Publishing, Houston, fifth edition edition, 1997. doi: https://doi.org/10.1016/B978-088415220-0/50002-1.

[26] Paul H.M. Feron, Ashleigh Cousins, Kaiqi Jiang, Rongrong Zhai, and Monica Garcia. An update of the benchmark post-combustion co2-capture technology. *Fuel*, 273, 8 2020. ISSN 00162361. doi: 10.1016/j.fuel.2020.117776.

[27] Viga Rajiman, Hairul Nazirah Abdul Halim, Azmi Mohd Shariff, Muhammad Zubair Shahid, Abdulhalim Shah Maulud, Kok Keong Lau, and Lian See Tan. Co2 absorption from biogas using piperazine-promoted 2-amino-2-methyl-1-propanol: Process performance in a packed column. *Sustainability (Switzerland)*, 14, 6 2022. ISSN 20711050. doi: 10.3390/su14127095.

[28] Danlu Tong, Geoffrey C. Maitland, Martin J.P. Trusler, and Paul S. Fennell. Solubility of carbon dioxide in aqueous blends of 2-amino-2-methyl-1-propanol and piperazine. *Chemical Engineering Science*, 101:851–864, 9 2013. ISSN 0009-2509. doi: 10.1016/J.CES.2013.05.034.

[29] G.T. Rochelle. 3 - conventional amine scrubbing for co2 capture. In Paul H.M. Feron, editor, *Absorption-Based Post-combustion Capture of Carbon Dioxide*. Woodhead Publishing, 2016. doi: https://doi.org/10.1016/B978-0-08-100514-9.00003-2.

[30] Le Li, Alexander K. Voice, Han Li, Omkar Namjoshi, Thu Nguyen, Yang Du, and Gary T. Rochelle. Amine blends using concentrated piperazine. *Energy Procedia*, 37:353–369, 1 2013. ISSN 1876-6102. doi: 10.1016/J.EGYPRO.2013.05.121.

[31] Ida M Bernhardsen and Hanna K Knuutila. A review of potential amine solvents for co2 absorption process: Absorption capacity, cyclic capacity and pka.

[32] Yuli Artanto, James Jansen, Pauline Pearson, Graeme Puxty, Aaron Cottrell, Erik Meuleman, and Paul Feron. Pilot-scale evaluation of amp/pz to capture co2 from flue gas of an australian brown coal–fired power station. *International Journal of Greenhouse Gas Control*, 20:189–195, 1 2014. ISSN 1750-5836. doi: 10.1016/J.IJGGC.2013.11.002.

[33] Graeme Puxty and Robert Rowland. Modeling co2 mass transfer in amine mixtures: Pz-amp and pz-mdea. *Environmental Science and Technology*, 45:2398–2405, 3 2011. ISSN 0013936X. doi: 10.1021/es1022784.

[34] P. Brúder, A. Grimstvedt, T. Mejdell, and H.F Svendsen. Co2 capture into aqueous solutions of piperazine activated 2-amino-2-methyl-1-propanol. *Chemical Engineering Science*, 66:6193–6198, 2011. ISSN 0009-2509. doi: 10.1016/j.ces.2011.08.051.

[35] Arthur L. Kohl and Richard B. Nielsen. Chapter 9 - liquid phase oxidation processes for hydrogen sulfide removal. In Arthur L. Kohl and Richard B.

Nielsen, editors, *Gas Purification (Fifth Edition)*, pages 731–865. Gulf Professional Publishing, Houston, fifth edition edition, 1997. ISBN 978-0-88415-220-0. doi: https://doi.org/10.1016/B978-088415220-0/50009-4. URL https://www.sciencedirect.com/science/article/pii/B9780884152200500094.

[36] Shuiping Yan, Qingyao He, Shuaifei Zhao, Hong Zhai, Minhui Cao, and Ping Ai. Co2 removal from biogas by using green amino acid salts: Performance evaluation. *Fuel Processing Technology*, 129:203–212, 1 2015. ISSN 0378-3820. doi: 10.1016/J.FUPROC.2014.09.019.

[37] Muhammad Shuaib Shariff Azmi Mohd and Shaikh. *Aqueous Amino Acid Salts and Their Blends as Efficient Absorbents for CO2 Capture*. Springer International Publishing, 2017. ISBN 978-3-319-47262-1. doi: 10.1007/978-3-319-47262-1_6. URL https://doi.org/10.1007/978-3-319-47262-1_6.

[38] P S Kumar, J A Hogendoorn, G F Versteeg, and P H M Feron. *AIChE Journal*, 49, 2003. doi: https://doi.org/10.1002/aic.690490118. URL https://aiche.onlinelibrary.wiley.com/doi/abs/10.1002/aic.690490118.

[39] Fouad R.H. Abdeen, Maizirwan Mel, Mohammed Saedi Jami, Sany Izan Ihsan, and Ahmad Faris Ismail. A review of chemical absorption of carbon dioxide for biogas upgrading. *Chinese Journal of Chemical Engineering*, 24:693–702, 6 2016. ISSN 10049541. doi: 10.1016/j.cjche.2016.05.006.

[40] Nuzhat Muntaha, Mahmudul I. Rain, Lipiar K.M.O. Goni, Md Aftab Ali Shaikh, Mohammad S. Jamal, and Mosharof Hossain. A review on carbon dioxide minimization in biogas upgradation technology by chemical absorption processes. *ACS Omega*, 7:33680–33698, 9 2022. ISSN 24701343. doi: 10.1021/acsomega.2c03514.

[41] Arthur L. Kohl and Richard B. Nielsen. Alkaline salt solutions for acid gas removal. *Gas Purification*, pages 330–414, 1 1997. doi: 10.1016/B978-088415220-0/50005-7.

[42] Tobias Jockenhoevel, Ruediger Schneider, and Helmut Rode. Development of an economic post-combustion carbon capture process. *Energy Procedia*, 1:1043–1050, 2 2009. ISSN 1876-6102. doi: 10.1016/J.EGYPRO.2009.01.138.

[43] Berthold U. Melcher, Albert E. Reichl, Ralph Joh, Markus Kinzl, and Ansgar Kursawe. Validation, operation and smart full-scale design of an efficient reclaiming system for carbon capture solvents based on amino acid salt. *Energy Procedia*, 63:676–686, 2014. ISSN 1876-6102. doi: https://doi.org/10.

1016/j.egypro.2014.11.075. URL https://www.sciencedirect.com/science/article/pii/S1876610214018906. 12th International Conference on Greenhouse Gas Control Technologies, GHGT-12.

[44] Stefania Moioli, Laura A. Pellegrini, Minh T. Ho, and Dianne E. Wiley. A comparison between amino acid based solvent and traditional amine solvent processes for co2 removal. *Chemical Engineering Research and Design*, 146: 509–517, 6 2019. ISSN 0263-8762. doi: 10.1016/J.CHERD.2019.04.035. URL https://www.sciencedirect.com/science/article/pii/S0263876219302011.

[45] L. V. van der Ham, E. L.V. Goetheer, E. Sanchez Fernandez, M. R.M. Abu-Zahra, and T. J.H. Vlugt. Precipitating amino acid solutions. *Absorption-Based Post-Combustion Capture of Carbon Dioxide*, pages 103–119, 1 2016. doi: 10.1016/B978-0-08-100514-9.00005-6.

[46] R.D. Deshmukh and A.E. Mather. A mathematical model for equilibrium solubility of hydrogen sulfide and carbon dioxide in aqueous alkanolamine solutions. *Chemical Engineering Science*, 36(2), 1981. doi: https://doi.org/10.1016/0009-2509(81)85015-4.

[47] Markus Rabensteiner, Gerald Kinger, Martin Koller, Günter Gronald, Sven Unterberger, and Christoph Hochenauer. Investigation of the suitability of aqueous sodium glycinate as a solvent for post combustion carbon dioxide capture on the basis of pilot plant studies and screening methods. *International Journal of Greenhouse Gas Control*, 29:1–15, 10 2014. ISSN 1750-5836. doi: 10.1016/J.IJGGC.2014.07.011.

[48] Ugochukwu E. Aronu, Arlinda F. Ciftja, Inna Kim, and Ardi Hartono. Understanding precipitation in amino acid salt systems at process conditions. *Energy Procedia*, 37:233–240, 1 2013. ISSN 1876-6102. doi: 10.1016/J.EGYPRO.2013.05.107.

[49] Bikash K. Mondal, Syamalendu S. Bandyopadhyay, and Amar N. Samanta. Vle of co2 in aqueous sodium glycinate solution - new data and modeling using kent-eisenberg model. *International Journal of Greenhouse Gas Control*, 36: 153–160, 5 2015. ISSN 17505836. doi: 10.1016/j.ijggc.2015.02.010.

[50] Faisal Harris, Kiki Adi Kurnia, M.Ibrahim A. Mutalib, and Murugesan Thanapalan. Solubilities of carbon dioxide and densities of aqueous sodium glycinate solutions before and after co2 absorption. *Journal of Chemical & amp; Engineering Data*, 54:144–147, 12 2008. doi: 10.1021/je800672r.

[51] A. Hartono, R. Ahmad, H.F. Svendsen, and H.K. Knuutila. New solubility and heat of absorption data for co2 in blends of 2-amino-2-methyl-1-panol (amp) and piperazine (pz) and a new enrtl model representation. *Fluid Phase Equilibria*, 550:113235, 2021. ISSN 0378-3812. doi: https://doi.org/10.1016/j.fluid.2021.113235. URL https://www.sciencedirect.com/science/article/pii/S0378381221002983.

[52] Ho Jun Song, Seungmoon Lee, Sanjeev Maken, Jong Jin Park, and Jin Won Park. Solubilities of carbon dioxide in aqueous solutions of sodium glycinate. *Fluid Phase Equilibria*, 246:1–5, 8 2006. ISSN 0378-3812. doi: 10.1016/J.FLUID.2006.05.012.

[53] A. F. Portugal, J. M. Sousa, F. D. Magalhães, and A. Mendes. Solubility of carbon dioxide in aqueous solutions of amino acid salts. *Chemical Engineering Science*, 64:1993–2002, 5 2009. ISSN 0009-2509. doi: 10.1016/J.CES.2009.01.036.

[54] Zih-Yi Yang, Allan N. Soriano, Alvin R. Caparanga, and Meng-Hui Li. Equilibrium solubility of carbon dioxide in (2-amino-2-methyl-1-propanol+piperazine+water). *The Journal of Chemical Thermodynamics*, 42(5):659–665, 2010. ISSN 0021-9614. doi: https://doi.org/10.1016/j.jct.2009.12.006. URL https://www.sciencedirect.com/science/article/pii/S0021961409003024.

[55] Ralph H Weiland, Nathan A Hatcher, and Jaime L Nava. Post-combustion co 2 capture with amino-acid salts. pages 22–24, 9 2010.

[56] Takashi Ogawa. Carbon dioxide capture and utilization for gas engine. *Energy and Power Engineering*, 05:587–590, 2013. ISSN 1949-243X. doi: 10.4236/epe.2013.510064.

[57] Y. Le Moullec and T. Neveux. 13 - process modifications for co2 capture. In Paul H.M. Feron, editor, *Absorption-Based Post-combustion Capture of Carbon Dioxide*, pages 305–340. Woodhead Publishing, 2016. ISBN 978-0-08-100514-9. doi: https://doi.org/10.1016/B978-0-08-100514-9.00013-5. URL https://www.sciencedirect.com/science/article/pii/B9780081005149000135.

[58] Finn Andrew Tobiesen, Geir Haugen, and Ardi Hartono. A systematic procedure for process energy evaluation for post combustion co2 capture: Case study of two novel strong bicarbonate-forming solvents. *Applied Energy*, 211:161–173, 2 2018. ISSN 0306-2619. doi: 10.1016/J.APENERGY.2017.10.091.

[59] Jacob Nygaard Knudsen, Jimmy Andersen, Jørgen Nørklit Jensen, and Ole Biede. Results from test campaigns at the 1 t/h co2 post-combustion capture pilot-plant in esbjerg under the eu fp7 cesar project. *ieaghg- PCCC1*.

[60] Hari Prasad Mangalapally and Hans Hasse. Pilot plant experiments for post combustion carbon dioxide capture by reactive absorption with novel solvents. *Energy Procedia*, 4:1–8, 2011. ISSN 1876-6102. doi: https://doi.org/10.1016/j.egypro.2011.01.015. URL https://www.sciencedirect.com/science/article/pii/S1876610211000166. 10th International Conference on Greenhouse Gas Control Technologies.

[61] Gavin Towler and Ray Sinnott. Capital cost estimating. *Chemical Engineering Design*, pages 307–354, 1 2013. doi: 10.1016/B978-0-08-096659-5.00007-9. URL https://linkinghub.elsevier.com/retrieve/pii/B9780080966595000079.

[62] Wallace Whiting, Joseph Shaeiwitz, Richard Turton, and Debangsu Bhattacharyya. Analysis, synthesis, and design of chemical processes. pages 951–969, 2018.

Appendix

The appendix contains the following sections:

A VLE-validation

B Economics

A VLE-validation data

Partial pressure of CO2 as a function of loading for the SG-CO2 system is presented below in Figures A.1, A.2, A.3, A.4, A.5 and A.6. The graphs have a weight percentage of 1, 5, 15, 20, 25 and 30 respectively.

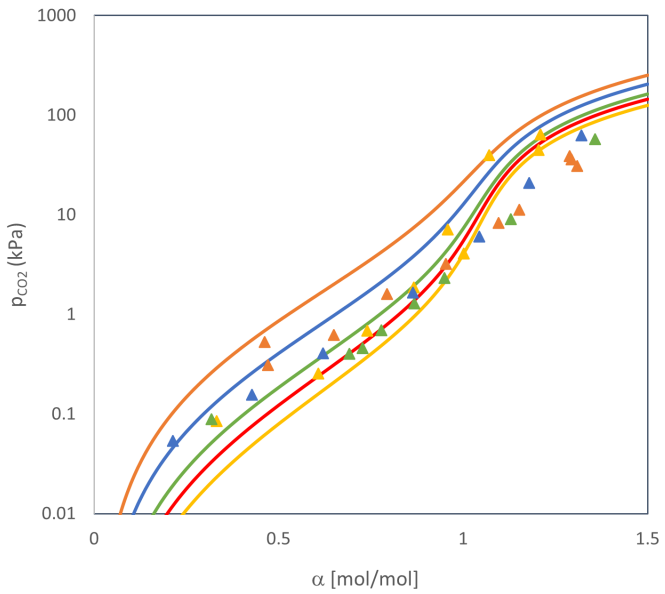

Figure A.1: Partial pressure of CO_2 as a function of CO_2 loading in 1 wt% SG at temperature between 20 and 50°C. The marker points correspond to the literature values: Song ●, Mondal ■, Harris ♦, Portugal ▲.

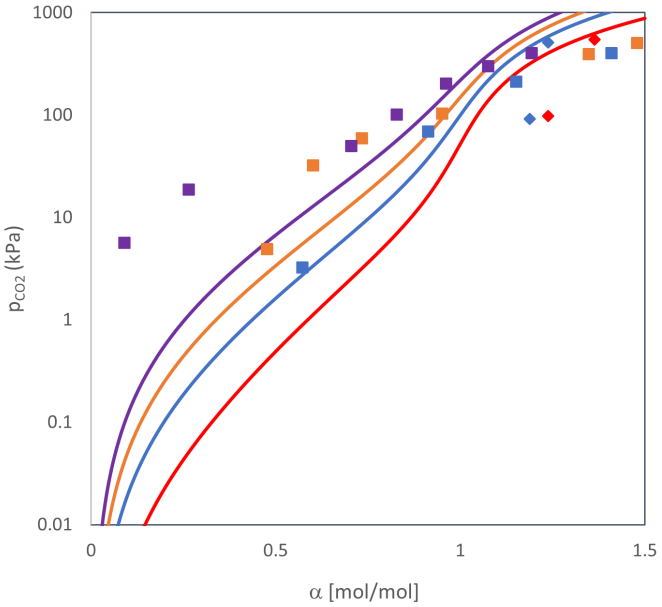

Figure A.2: Partial pressure of CO_2 as a function of CO_2 loading in 5 wt% SG at temperature between 25 and 60°C. The marker points correspond to the literature values: Song ●, Mondal ■, Harris ♦, Portugal ▲.

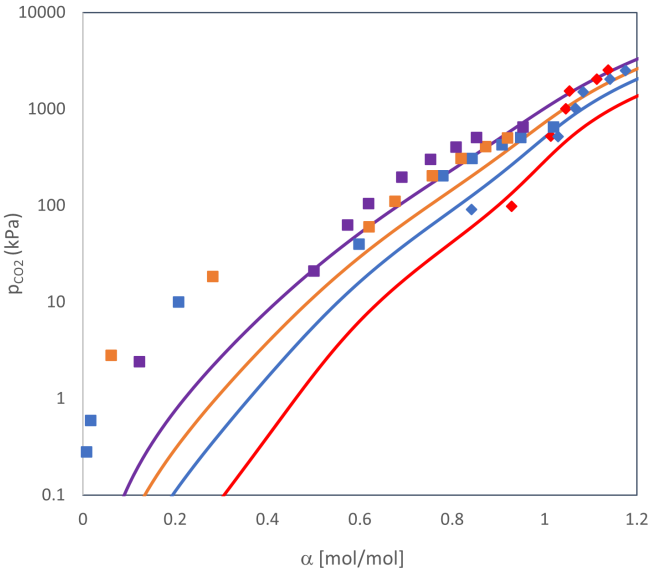

Figure A.3: Partial pressure of CO_2 as a function of CO_2 loading in 15 wt% SG at temperature between 25 and 60°C. The marker points correspond to the literature values: Song ●, Mondal ■, Harris ♦, Portugal ▲.

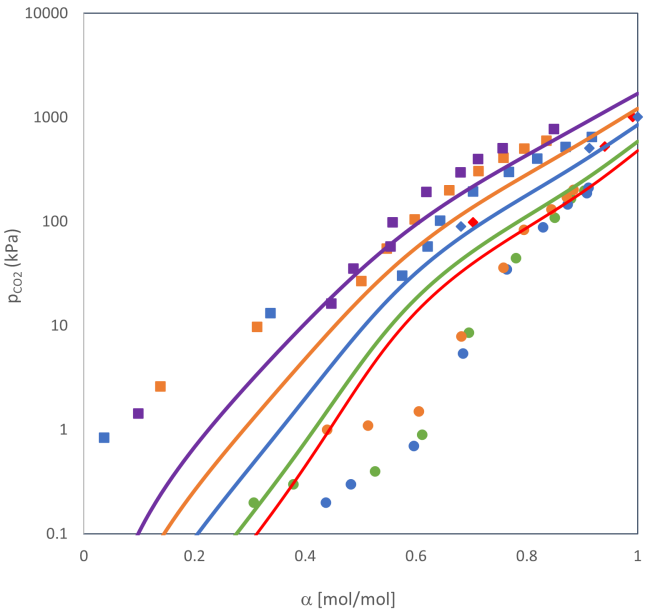

Figure A.4: Partial pressure of CO_2 as a function of CO_2 loading in 20 wt% SG at temperature between 25 and 60°C. The marker points correspond to the literature values: Song ●, Mondal ■, Harris ♦, Portugal ▲.

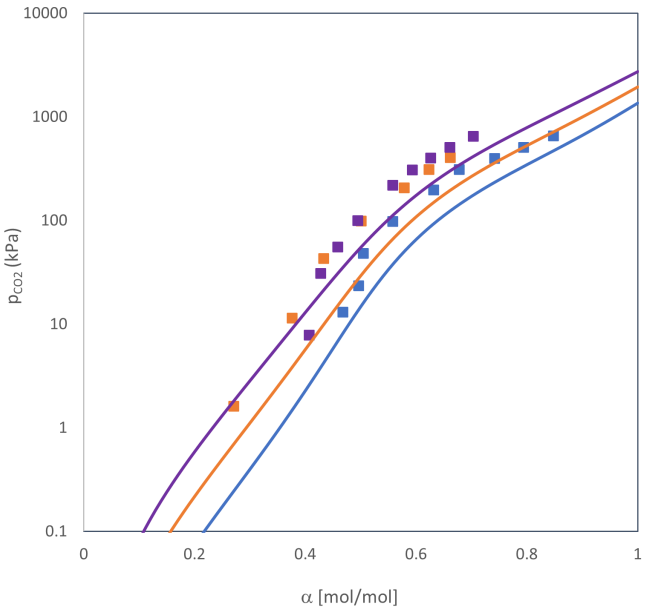

Figure A.5: Partial pressure of CO_2 as a function of CO_2 loading in 25 wt% SG at temperature between 40 and 60°C. The marker points correspond to the literature values: Song ●, Mondal ■, Harris ♦, Portugal ▲.

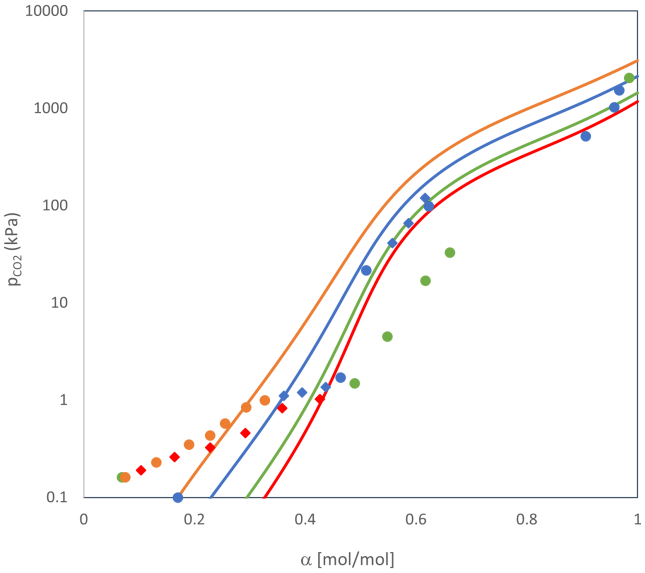

Figure A.6: Partial pressure of CO_2 as a function of CO_2 loading in 30 wt% SG at temperature between 25 and 50℃. The marker points correspond to the literature values: Song ●, Mondal ■, Harris ◆, Portugal ▲.

B Economics

Equipment cost

The equipment type used from the literature is shown in Table B.1. The parameters for sizing of the equipment are shown in Table B.2. For equation 7.1 CEPEI at 532.9 from 2010 was used. For equation 7.2 CEPEI at 397 from 2001 was used. To estimate the cost in toady's value a CEPEI of 720.2 for 2021 was used.

Table B.1: Equipment type used in the litterature to estimate cost

Equipment	**Equipment name in literature**
Absorber	Pressure vessel- vertical
Stripper	Pressure vessel- vertical
Packing	304ss structure packing
Reboiler	U-tube Kettle boiler Pressure vessel - horizontal 304 ss
Condenser	Exchangers- plate and frame pressure vessel- horizontal
HEX and coolers	Exchangers- plate and frame
Pumps	Pumps and drivers- single stage centrifugal
compressor	compressor- blower
flash	pressure vessel- vertical- 304ss

Table B.2: Parameters and units for estimating equipment cost in Equation 7.1 and 7.2

Equipment	Unit for size, S	a (K1)	b (K2)	n (K3)
Absorber	shell mass, kg	17400	79	0.85
Stripper	shell mass, kg	17400	79	0.85
Packing	volume, m^3	-	7600	1
Reboiler	area, m^2	29000	400	0.9
	shell mass, kg	12800	73	0.85
Condenser	area, m^2	1600	210	0.95
	volume, m^3	3.5565	0.3776	0.0905
HEX and coolers	area, m^2	1600	210	0.95
Pumps	flow, liters/s	8000	240	0.9
compressor	m^3/h	4450	57	0.8
flash	shell mass, kg	17400	79	0.85

Factorial method

The factorial method was used to estimate the ISBL from equipment costs. Items and values for the variables in Equation 7.3, 7.4 and 7.5 and are shown in Table B.3.

Table B.3: Values used in the factoril method in Equations 7.3, 7.4 and 7.5

Item	Explanation	Value
f_{er}	equipment erection	0.3
f_p	piping	0.8
f_i	instrumentation and control	0.3
f_{el}	electrical	0.2
f_c	civil	0.3
f_s	structure and buildings	0.2
f_l	Lagging and paint	0.1
f_m(SS)	material cost factor SS 304	1.3
OS	offsites	0.3
D&E	design and Engineering	0.3
X	Contingency	0.1

Working capital and operational costs

The working capital was assumed to be 15% of ISBL. Operating costs was divided into fixed and variable costs. Table B.4 shows the values for fixed cost.

Table B.4: Values used to calculate fixed costs

Fixed costs	Explanation
Maintenance	5% of ISBL
Property taxes and insurance	2% of fix capital
Operators, no. of shifts	1 operator x3 shifts
Operator salaries	50000$/year
Supervision and management	25% of operating labour
Direct salary overhead	60% of operating labour
Research and development	15% of revenues
General and Administrative	65% of labour cost + supervision and overhead
Royalties	5% of revenues

To calculate the variable cost the parameters shown in Table B.5 were used.

Table B.5: Values used for calculating varaible costs

Variable costs	Value	Unit
Electricity	0.183	$/kWh
Steam	20.4	$/ton
Cooling water	0.07	$/tons
Amine	8.78	$/kg amine
Amine degradation	1.6	kg amine/ton CO2

Profitability analysis

The equation used to calculate the DNPV, PBT and IRR is:

$$V = \sum_{i=1}^{N} \frac{CF_i}{(1 + DR)^i} - INV_0 + RV_N \tag{B.1}$$

where V is the value of the investment/project, CF is the cash flow, DR is the discount rate, N is the number of periods of the time span of interest of the investment, INV_0 is the initial investment and RV_N is the residual value at nth period.

It was assumed 20% linear depreciation, 28% tax and a discount rate of 8%.

Economical results

Equipment cost found for each case is shown in Table B.6 and B.7.

Table B.6: Equipment cost for case 1, 2 and 3 in the economic analysis in USD

Equipment	Case 1	Case 2	Case 3
Absorber	124 287	112 945	91 672
Stripper	123 610	86 837	91 543
Reboiler	120 589	98 722	120 414
Condenser	15 172	9 955	15 224
HEX and coolers	118 775	76 984	118 655
Pumps	24 995	23 824	24 976
Compressor	42 915	42 915	42 915
Flash	33 341	33 230	33 304

Table B.7: Equipment cost for case 4, 5 and 6 in the economic analysis in USD

Equipment	**Case 4**	**Case 5**	**Case 6**
Absorber	93 139	84 908	84 099
Stripper	86 602	70 053	67 842
Reboiler	118 471	101 533	99 595
Condenser	14 045	10 659	10 998
HEX and coolers	99 773	83 459	79 308
Pumps	24 883	23 979	23 876
Compressor	42 915	42 915	42 915
Flash	26 309	33 230	33 229

NTNU

Norwegian University of
Science and Technology